Supplementary Material: Validation of turbulence models for predicting pressure coefficients for natural ventilation purposes on an isolated low-rise building.

Ángel Sánchez-Cruz[a], Eduardo Ramos[a], Edmundo Amaya-Gallardo[b], Vladimir Arturo Reyes Herrera[a], Saul Piedra[c]

[a] *Renewable Energy Institute, Universidad Nacional Autónoma de México (UNAM), Temixco, Mor., 62580, Mexico*
[b] *Civil Engineering Faculty, Universidad Autónoma de Coahuila (UAdeC), Torreón, Coah., 27275, Mexico*
[c] *SECIHTI - Centro de Ingeniería y Desarrollo Industrial, Querétaro, Qro., 76125, Mexico*

Abstract

This document is the supplementary material for the article titled "Validation of turbulence models for representing pressure coefficients for natural ventilation purposes on an isolated low-rise building". It provides further validation and analysis of turbulence models used to represent the pressure coefficients (C_P) on an isolated low-rise building, with the goal of assessing their applicability in natural ventilation design.

The validation includes velocity and turbulence profiles within a computational domain without any building structure, demonstrating that the velocity profiles (U) and turbulence variables (I, k, ϵ, ω) remain consistent across the domain. Additionally, contour maps of pressure coefficients on the building faces for various wind incidence angles are presented, obtained from CFD simulations. These results are compared to experimentally derived wall-averaged pressure coefficients.

The document also includes local comparisons of the pressure coefficients obtained from the BDA and TPU databases, with CFD simulations. The accuracy of the turbulence models is assessed through the Normalized Mean Square Error (NMSE) and the Normalized Root Mean Square Error (ε). Furthermore, the analysis extends to local pressure coefficients along the

horizontal and vertical centerlines of the building. Turbulent kinetic energy and turbulent viscosity fields are also examined, along with comparisons of flow streamlines for different wind incidence angles.

Overall, this supplementary material provides a comprehensive evaluation of the turbulence models and their effectiveness in predicting pressure coefficients within the context of natural ventilation in buildings.

---

1. Validation of Profiles Through Domain, Pressure Coefficient Contour Maps and Qualitative Assessment of Wall-Averaged Pressure Coefficient

Section 1.1 presents the validation of the velocity and turbulence profiles within the computational domain without building. These profiles were sampled at five distinct points, spanning from the inlet to the outlet of the *empty* domain. The theoretical velocity profile, u, is plotted to demonstrate that it traverses the domain without perturbations, ensuring that the turbulence profiles, I, k, ϵ, and ω, remain consistent throughout.

Section 1.2 presents the contour maps of pressure coefficients on the building faces for atmospheric boundary layer profile incidence angles of 0°, 15°, 30°, and 45°, derived from CFD simulations. The contour maps include results obtained using the STD k-ϵ, Realizable k-ϵ, RNG k-ϵ, STD k-ω, and SST k-ω turbulence models.

Section 1.3 presents a qualitative analysis of the wall-averaged pressure coefficient ($\overline{C_P}$), comparing the CFD results from this study with experimental data.

1.1. Velocity and Turbulence Profiles Through Domain

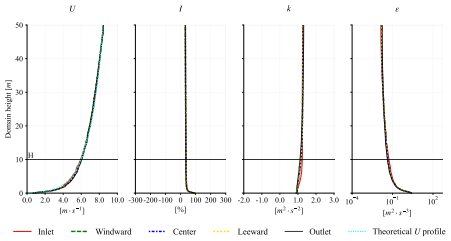

(a) 0°

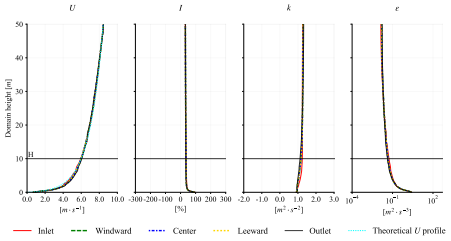

(b) 15°

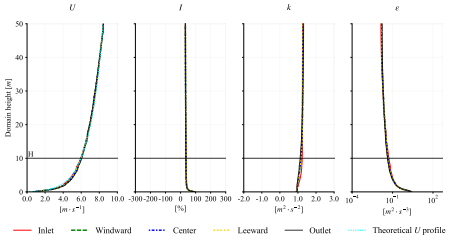

(c) 30°

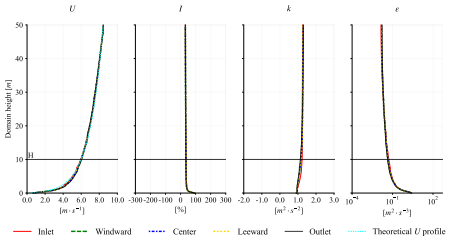

(d) 45°

Figure 1: Velocity and turbulent profiles, STD k-ϵ for the sampling locations through the domain. Building height (H) equals to reference height (y_{ref}), for the ABL setup.

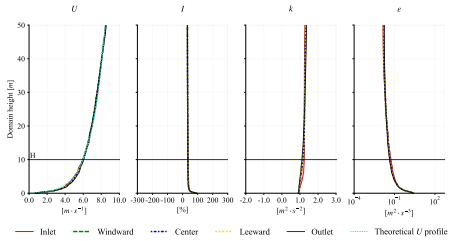

(a) 0°

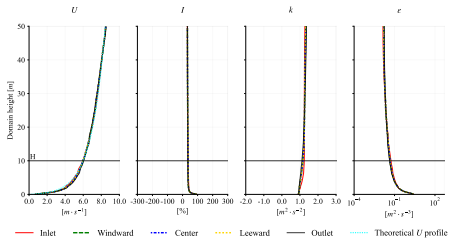

(b) 15°

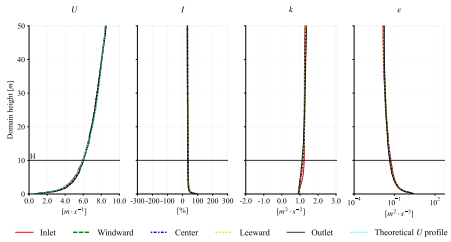

(c) 30°

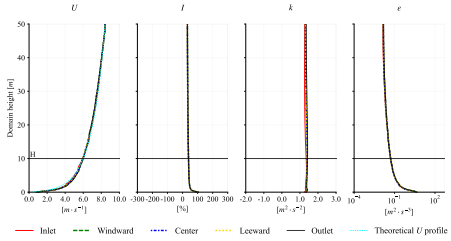

(d) 45°

Figure 2: Velocity and turbulent profiles, Realizable k-ϵ for the sampling locations through the domain. Building height (H) equals to reference height (y_{ref}), for the ABL setup.

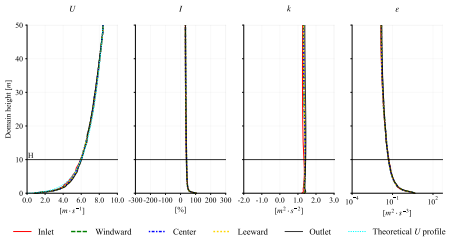

(a) 0°

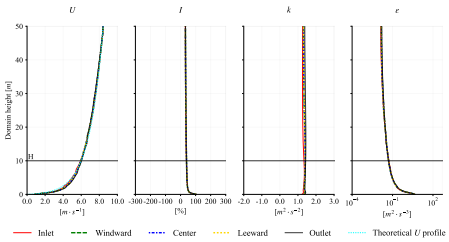

(b) 15°

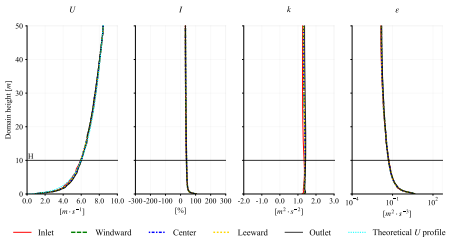

(c) 30°

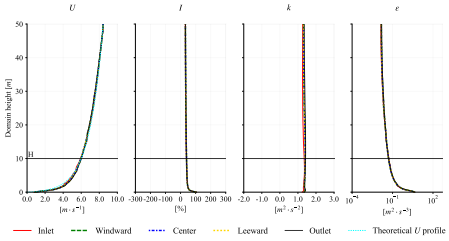

(d) 45°

Figure 3: Velocity and turbulent profiles, RNG k-ϵ for the sampling locations through the domain. Building height (H) equals to reference height (y_{ref}), for the ABL setup.

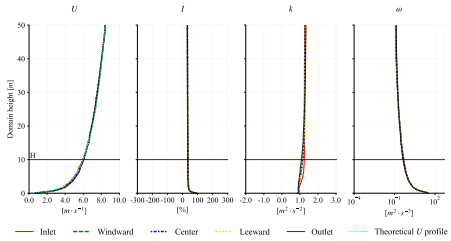

(a) 0°

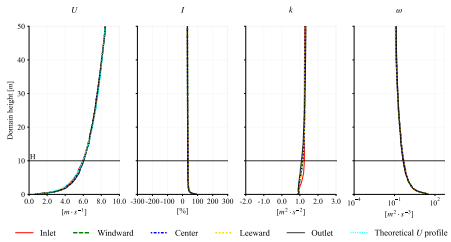

(b) 15°

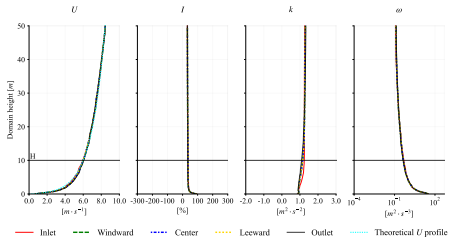

(c) 30°

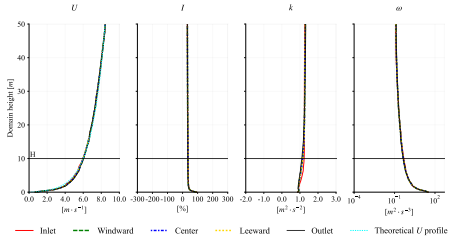

(d) 45°

Figure 4: Velocity and turbulent profiles, STD k-ω for the sampling locations through the domain. Building height (H) equals to reference height (y_{ref}), for the ABL setup.

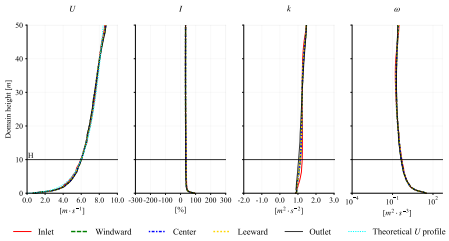

(a) 0°

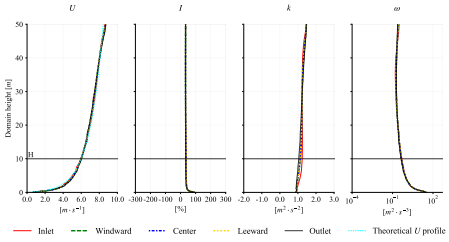

(b) 15°

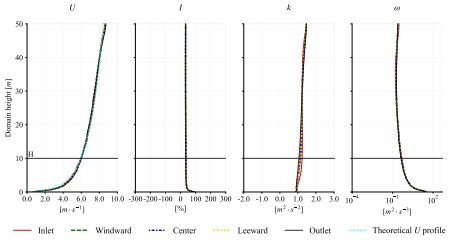

(c) 30°

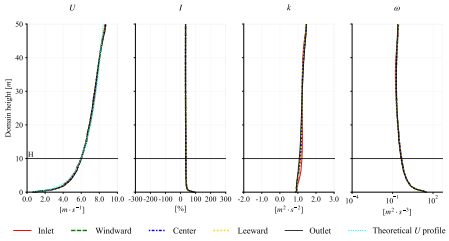

(d) 45°

Figure 5: Velocity and turbulent profiles, SST k-ω for the sampling locations through the domain. Building height (H) equals to reference height (y_{ref}), for the ABL setup.

1.2. Contour Maps of Pressure Coefficients Derived from CFD Simulations

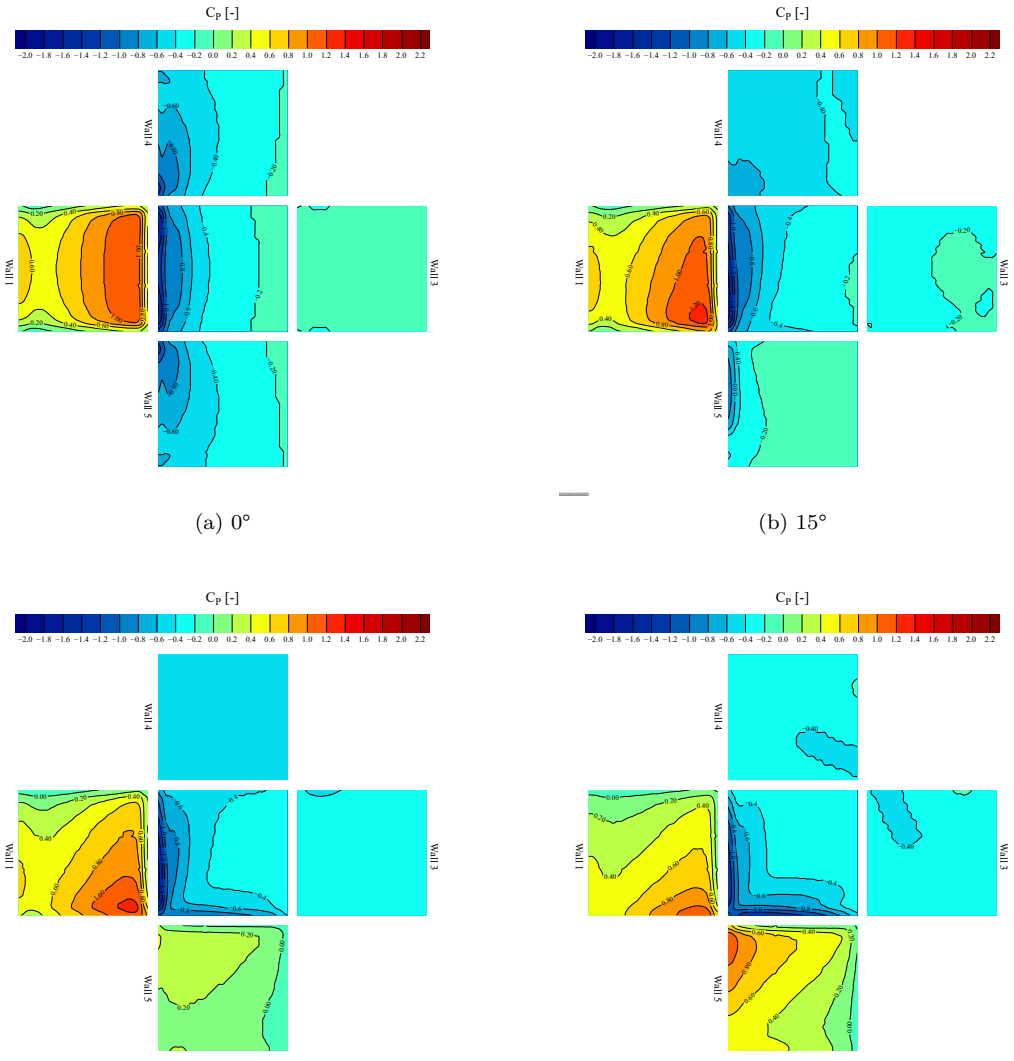

(a) 0°

(b) 15°

(c) 30°

(d) 45°

Figure 6: C_P contour maps, STD k-ϵ

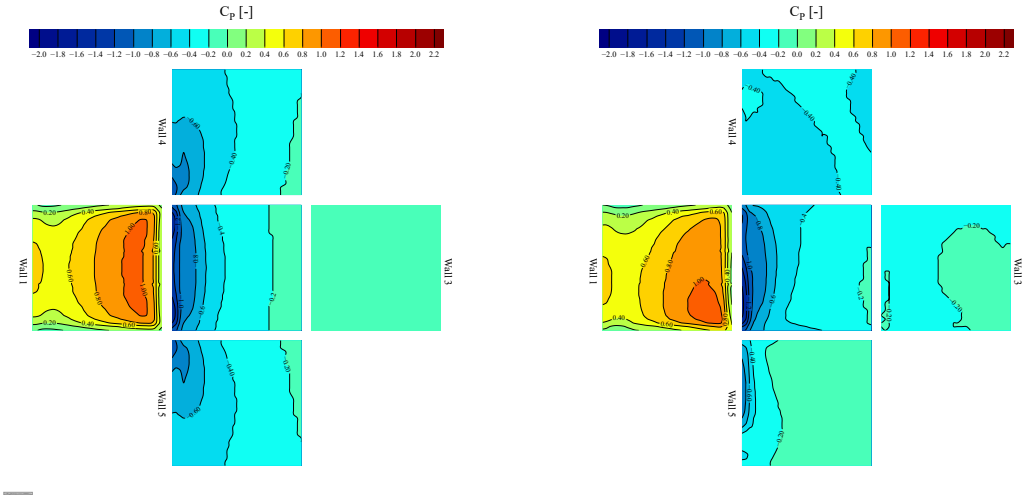

(a) 0°

(b) 15°

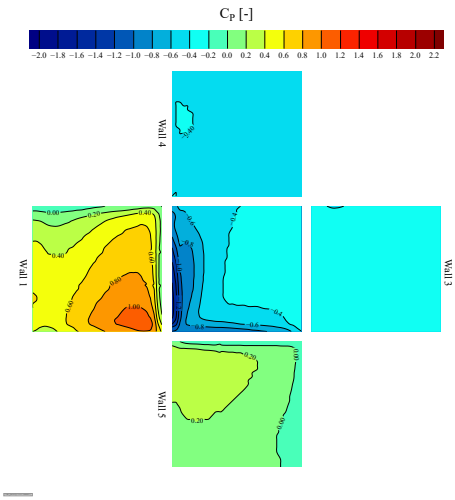

(c) 30°

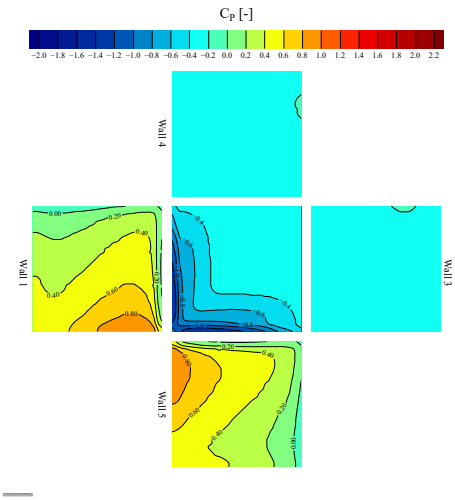

(d) 45°

Figure 7: C_P contour maps, Realizable k-ϵ

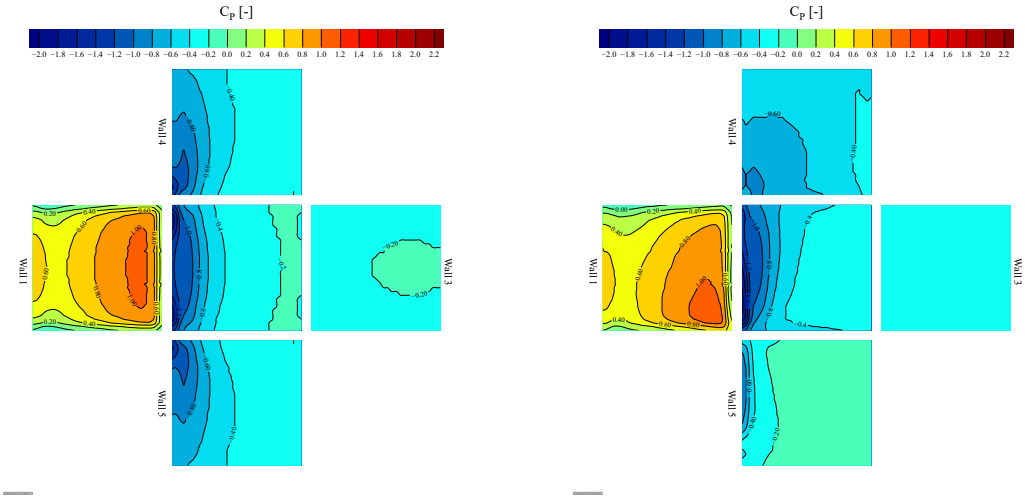

(a) 0°

(b) 15°

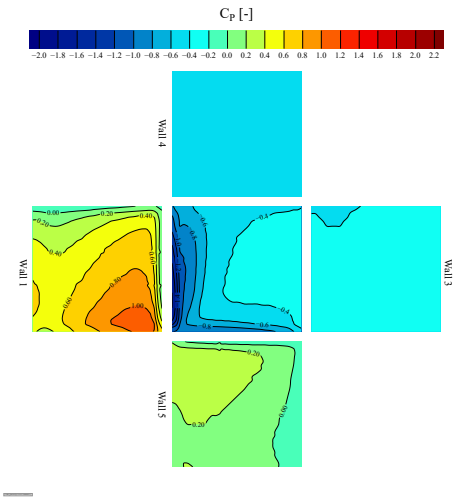

(c) 30°

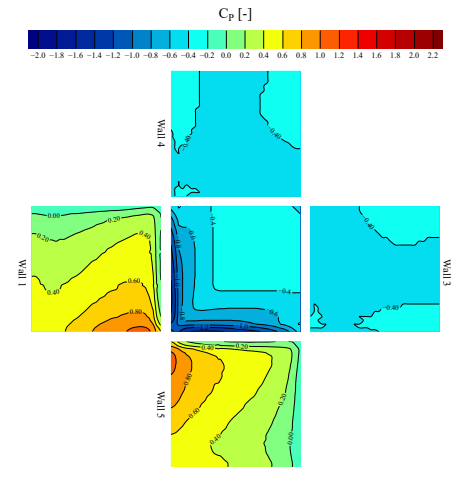

(d) 45°

Figure 8: C_P contour maps, RNG k-ϵ

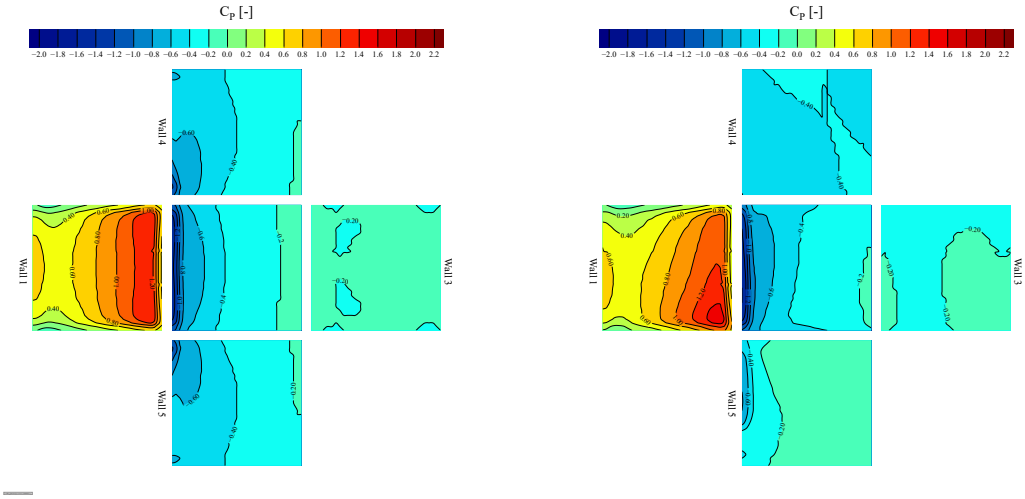

(a) 0°

(b) 15°

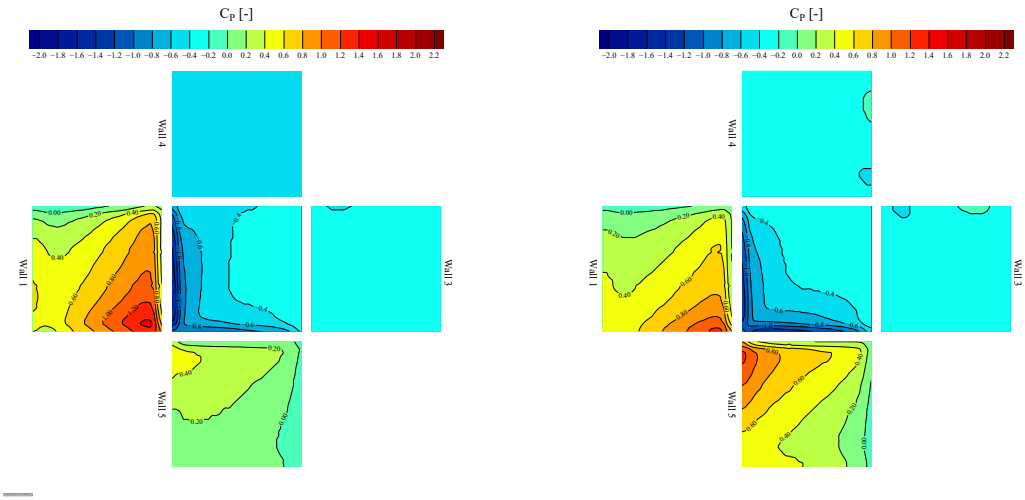

(c) 30°

(d) 45°

Figure 9: C_P contour maps, STD k-ω

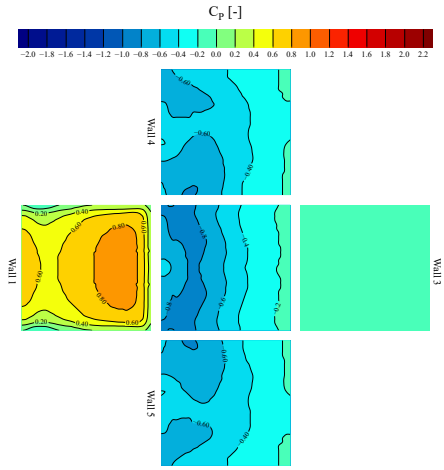

(a) 0°

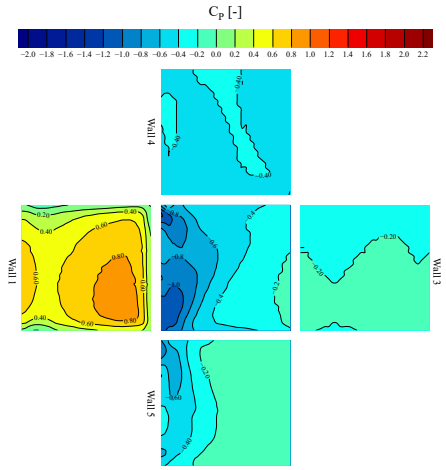

(b) 15°

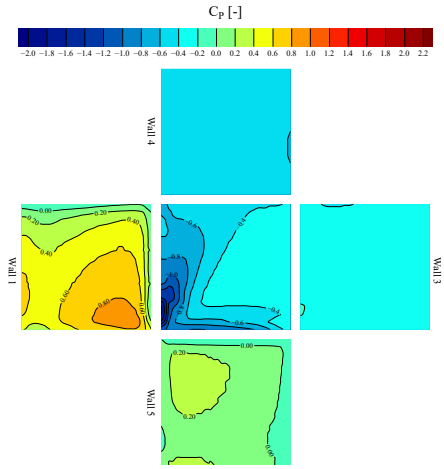

(c) 30°

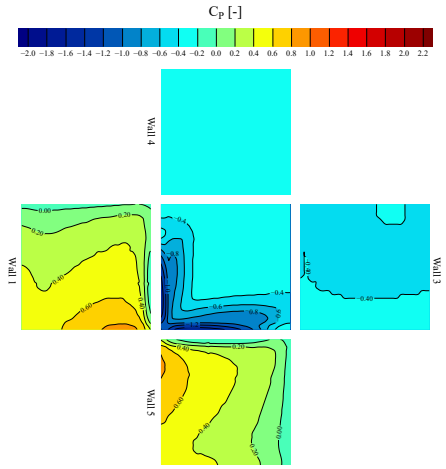

(d) 45°

Figure 10: C_P contour maps, SST k-ω

1.3. Quantitative analysis of wall-averaged pressure coefficient $\overline{C_P}$

Table 1 presents the averaged pressure coefficient ($\overline{C_P}$) over the entire surface, based on the available database information and the studied k-ϵ and k-ω turbulence models.

Table 2 presents the relative error (ε_r), calculated using Equation (1), based on the values from Table 1.

$$\varepsilon_r = 100 \left| \frac{\varphi_{(x=0)} - \varphi_{(x)}}{\varphi_{(x=0)}} \right| \tag{1}$$

where $\varphi_{(x=0)}$ represents the *reference value*, and $\varphi_{(x)}$ denotes the *computed value*.

For the calculation of ε_r in Table 2, the AIVC dataset was used as the reference value $\varphi_{(x=0)}$.

Yellow and green cells indicate the smallest and second smallest ε_r values, respectively, for the turbulence models. The BDA and TPU ε_r values are included as reference.

Following the same methodology as in Table 2, Tables 3 and 4 present the smallest and second smallest wall-averaged pressure coefficient ($\overline{C_P}$) relative error (ε_r) for the studied turbulence models, considering the BDA and TPU databases as reference values, respectively.

Table 1: Comparison of $\overline{C_P}$ on the walls. Databases, k-ϵ and k-ω turbulence models

Database / Model	**Wind incidence**	**Wall 1**	**Wall 2**	**Wall 3**	**Wall 4**	**Wall 5**
AIVC	0°	0.70	-	-0.20	-0.50	-0.50
BDA	0°	0.73	-0.74	-0.31	-0.65	-0.69
TPU	0°	0.68	-0.84	-0.35	-0.77	-0.75
k-ϵ STD	0°	0.69	-0.44	-0.18	-0.41	-0.41
k-ϵ Realizable	0°	0.64	-0.44	-0.17	-0.41	-0.41
k-ϵ RNG	0°	0.64	-0.47	-0.22	-0.44	-0.44
k-ω STD	0°	0.74	-0.43	-0.18	-0.40	-0.40
k-ω SST	0°	0.58	-0.53	-0.16	-0.47	-0.47
TPU	15°	0.63	-0.74	-0.36	-0.74	-0.37
k-ϵ STD	15°	0.67	-0.48	-0.22	-0.46	-0.18
k-ϵ Realizable	15°	0.63	-0.48	-0.22	-0.42	-0.19
k-ϵ RNG	15°	0.62	-0.52	-0.27	-0.55	-0.19
k-ω STD	15°	0.72	-0.46	-0.22	-0.44	-0.17
k-ω SST	15°	0.56	-0.52	-0.21	-0.43	-0.22
BDA	30°	0.61	-0.72	-0.49	-0.72	0.01
TPU	30°	0.53	-0.70	-0.44	-0.70	0.10
k-ϵ STD	30°	0.58	-0.52	-0.28	-0.48	0.14
k-ϵ Realizable	30°	0.55	-0.51	-0.27	-0.44	0.13
k-ϵ RNG	30°	0.55	-0.56	-0.34	-0.53	0.13
k-ω STD	30°	0.62	-0.51	-0.27	-0.46	0.16
k-ω SST	30°	0.48	-0.51	-0.26	-0.46	0.10
AIVC	45°	0.35	-	-0.40	-0.40	0.35
BDA	45°	0.40	-0.71	-0.61	-0.60	0.32
TPU	45°	0.33	-0.63	-0.52	-0.53	0.34
k-ϵ STD	45°	0.43	-0.49	-0.35	-0.35	0.43
k-ϵ Realizable	45°	0.40	-0.49	-0.31	-0.31	0.40
k-ϵ RNG	45°	0.40	-0.54	-0.41	-0.41	0.40
k-ω STD	45°	0.45	-0.49	-0.32	-0.32	0.45
k-ω SST	45°	0.36	-0.49	-0.41	-0.26	0.32

Table 2: Wall $\overline{C_P}$ relative error with respect to AIVC database

Database / Turbulence model	**Wind incidence**	**Wall 1** [%]	**Wall 2** [%]	**Wall 3** [%]	**Wall 4** [%]	**Wall 5** [%]
AIVC	0°	*	*	*	*	*
BDA	0°	4.29	*	55.00	30.00	38.00
TPU	0°	2.86	*	75.00	54.00	50.00
k-ϵ STD	0°	1.43	*	10.00	18.00	18.00
k-ϵ Realizable	0°	8.57	*	15.00	18.00	18.00
k-ϵ RNG	0°	8.57	*	10.00	12.00	12.00
k-ω STD	0°	5.71	*	10.00	20.00	20.00
k-ω SST	0°	17.14	*	20.00	6.00	6.00
AIVC	45°	*	*	*	*	*
BDA	45°	14.29	*	52.50	50.00	8.57
TPU	45°	5.71	*	30.00	32.50	2.86
k-ϵ STD	45°	22.86	*	12.50	12.50	22.86
k-ϵ Realizable	45°	14.29	*	22.50	22.50	14.29
k-ϵ RNG	45°	14.29	*	2.50	2.50	14.29
k-ω STD	45°	28.57	*	20.00	20.00	28.57
k-ω SST	45°	2.86	*	2.50	35.00	8.57

Table 3: Wall $\overline{C_P}$ relative error with respect to BDA database

Turbulence model	**Wind incidence**	**Wall 1** [%]	**Wall 2** [%]	**Wall 3** [%]	**Wall 4** [%]	**Wall 5** [%]
k-ϵ STD	0°	10.96	37.84	41.94	36.92	40.58
k-ϵ Realizable	0°	17.81	37.84	45.16	36.92	40.58
k-ϵ RNG	0°	19.18	33.78	25.81	27.69	31.88
k-ω STD	0°	1.37	37.84	41.94	38.46	42.03
k-ω SST	0°	26.03	29.73	48.39	29.23	33.33
k-ϵ STD	30°	6.56	25.00	40.82	33.33	1200.00
k-ϵ Realizable	30°	14.75	26.39	44.90	38.89	1000.00
k-ϵ RNG	30°	13.11	19.44	30.61	26.39	1000.00
k-ω STD	30°	0.00	26.39	44.90	36.11	1400.00
k-ω SST	30°	26.23	26.39	46.94	36.11	800.00
k-ϵ STD	45°	5.00	28.17	44.26	43.33	31.25
k-ϵ Realizable	45°	5.00	29.58	50.82	50.00	18.75
k-ϵ RNG	45°	5.00	21.13	32.79	31.67	18.75
k-ω STD	45°	12.50	28.17	49.18	48.33	40.63
k-ω SST	45°	12.50	29.58	32.79	56.67	3.13

Table 4: Wall $\overline{C_P}$ relative error with respect to TPU database

Turbulence model	**Wind incidence**	**Wall 1** [%]	**Wall 2** [%]	**Wall 3** [%]	**Wall 4** [%]	**Wall 5** [%]
k-ϵ STD	0°	8.82	50.00	48.57	46.75	45.33
k-ϵ Realizable	0°	1.47	48.81	51.43	48.05	46.67
k-ϵ RNG	0°	1.47	45.24	34.29	41.56	40.00
k-ω STD	0°	17.65	50.00	48.57	48.05	46.67
k-ω SST	0°	10.29	35.71	54.29	38.96	37.33
k-ϵ STD	15°	14.29	39.19	38.89	37.84	54.05
k-ϵ Realizable	15°	6.35	37.84	41.67	43.24	51.35
k-ϵ RNG	15°	6.35	33.78	25.00	25.68	51.35
k-ω STD	15°	23.81	40.54	41.67	40.54	54.05
k-ω SST	15°	6.35	29.73	41.67	41.89	40.54
k-ϵ STD	30°	16.98	31.43	36.36	31.43	60.00
k-ϵ Realizable	30°	9.43	31.43	38.64	37.14	40.00
k-ϵ RNG	30°	9.43	25.71	22.73	24.29	40.00
k-ω STD	30°	24.53	31.43	38.64	34.29	70.00
k-ω SST	30°	3.77	30.00	40.91	34.29	10.00
k-ϵ STD	45°	36.36	26.98	34.62	35.85	32.35
k-ϵ Realizable	45°	27.27	26.98	40.38	41.51	20.59
k-ϵ RNG	45°	27.27	20.63	21.15	22.64	20.59
k-ω STD	45°	42.42	26.98	40.38	39.62	38.24
k-ω SST	45°	15.15	28.57	21.15	52.83	0.00

2. Local CFD Pressure Coefficient Comparison with BDA and TPU Databases

Since the BDA and TPU databases provide tap coordinates and C_P values, it is possible to perform a *local* comparison for each tap position, even though the experimental and CFD cases were conducted at different scales. Figure 11 shows the experimental pressure tap positions for the BDA and TPU studies. In the BDA study, 125 pressure taps were used, with 25 taps arranged equidistantly on each wall (Figure 11a). In contrast, the TPU study used 284 pressure taps, with wall 2 having 64 equidistant taps, while the other walls had 55 taps arranged in a specific pattern, as shown in Figure 11b.

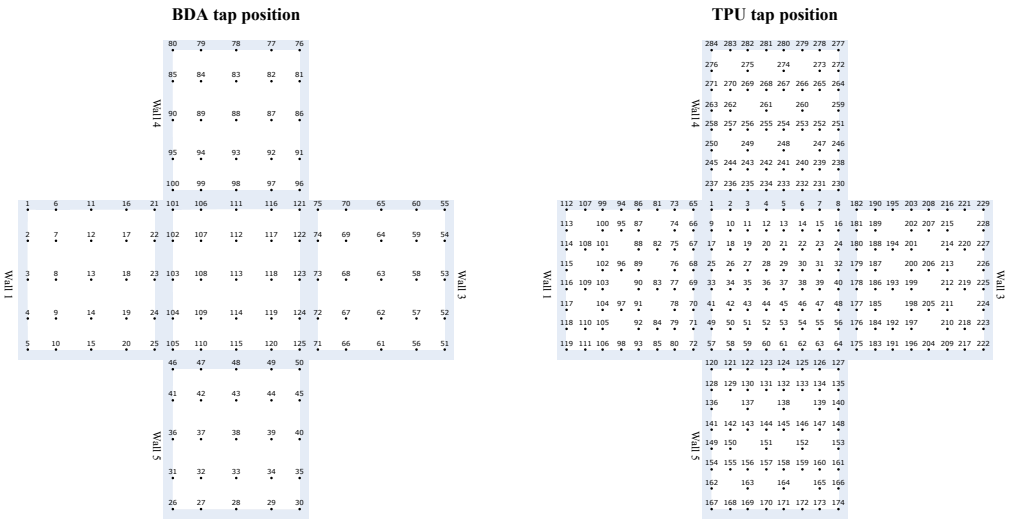

(a) BDA tap position

(b) TPU tap position

Figure 11: Experimental BDA and TPU tap position

Section 2.1 presents the contour maps derived from the experimental data of the BDA database, along with the corresponding CFD contour maps at the pressure tap coordinates provided by the database. Section 2.2 presents a similar set of contour maps for the TPU database.

Section 2.3 evaluates the accuracy of the turbulence models by comparing them with experimental data from the BDA and TPU databases. The analysis considers all walls, the wind incidence angles available from experimental

observations, and all turbulence models tested in this study.

Section 2.4 presents a qualitative analysis of the local pressure coefficients along the horizontal and vertical center-lines of the building. The analysis considers wind incidence angles of 0°, 15°, 30°, and 45°, and the results are compared with experimental data from the BDA and TPU datasets.

Section 2.5 presents the turbulent kinetic energy and turbulent viscosity fields on parallel and cross-sectional planes relative to the ABL angle of attack.
Section 2.6 qualitatively compares the streamlines in the top view, formed by the wind flow at 0°, 15°, 30°, and 45° for all the turbulence models studied. The objective is to identify differences in the recirculation and flow separation patterns for each turbulence model.

2.1. Pressure Coefficient Contour Maps. BDA vs CFD

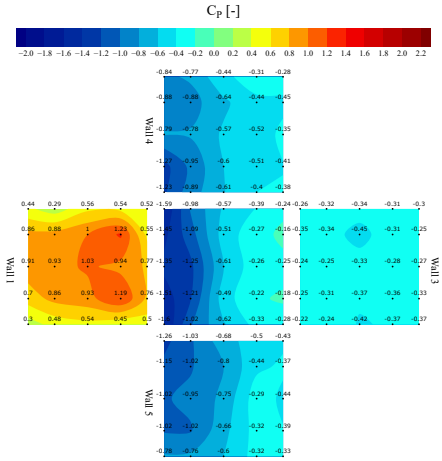

Figure 12: C_P contour maps, BDA 0°

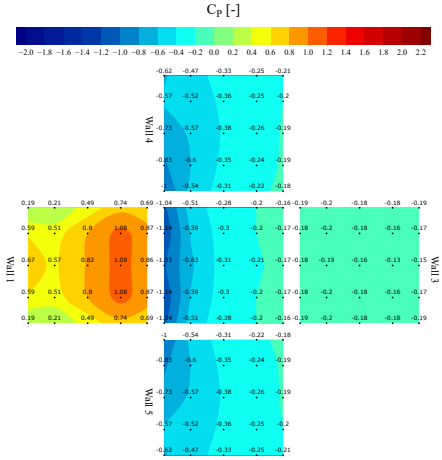

Figure 13: C_P contour maps at BDA tap coordinates, STD k-ϵ, 0°

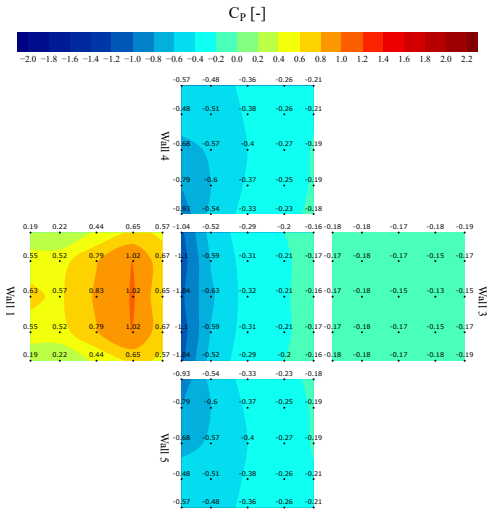

Figure 14: C_P contour maps at BDA tap coordinates, Realizable k-ϵ, 0°

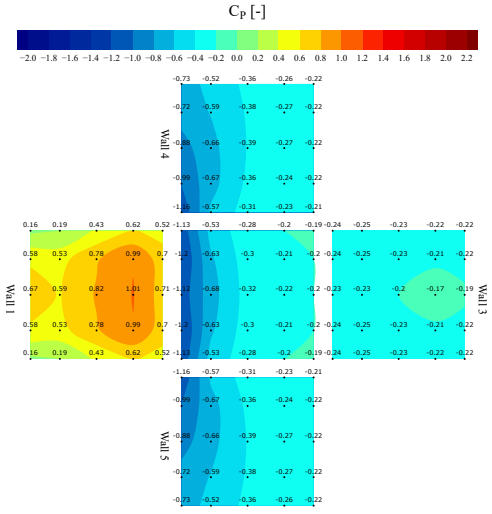

Figure 15: C_P contour maps at BDA tap coordinates, RNG k-ϵ, 0°

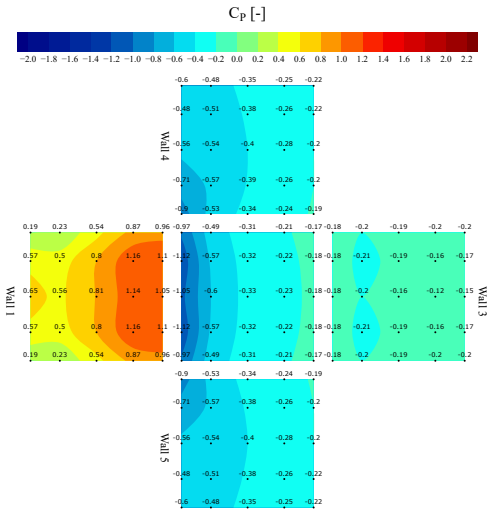

Figure 16: C_P contour maps at BDA tap coordinates, STD k-ω, 0°

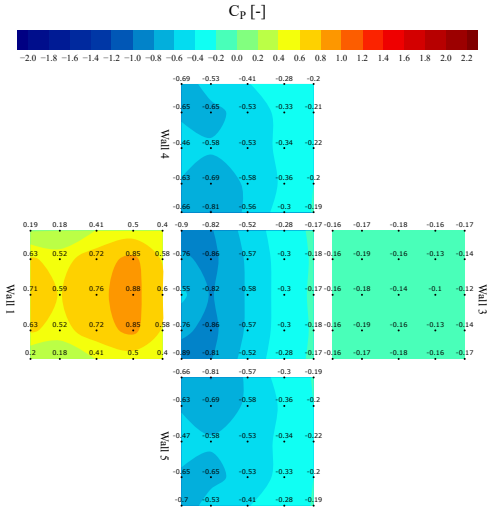

Figure 17: C_P contour maps at BDA tap coordinates, SST k-ω, 0°

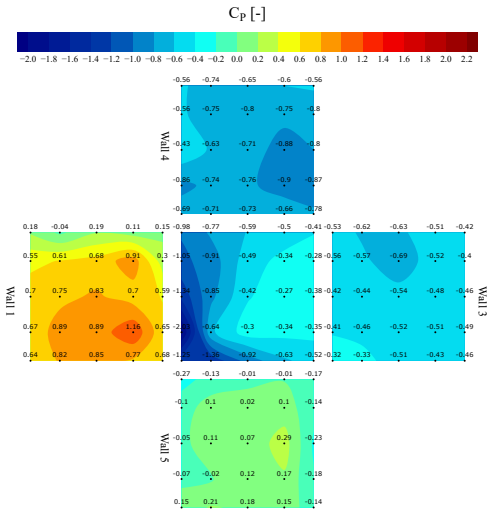

Figure 18: C_P contour maps, BDA 30°

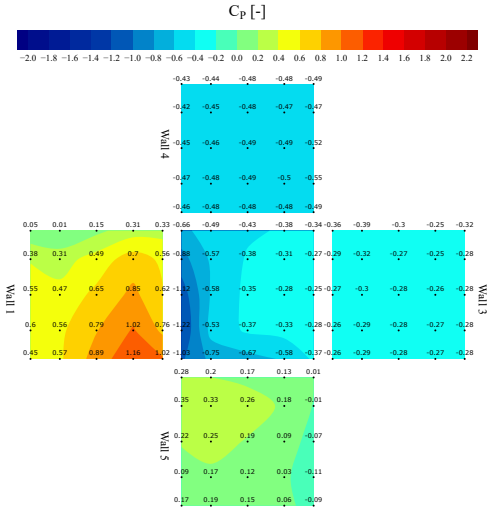

Figure 19: C_P contour maps at BDA tap coordinates, STD k-ϵ, 30°

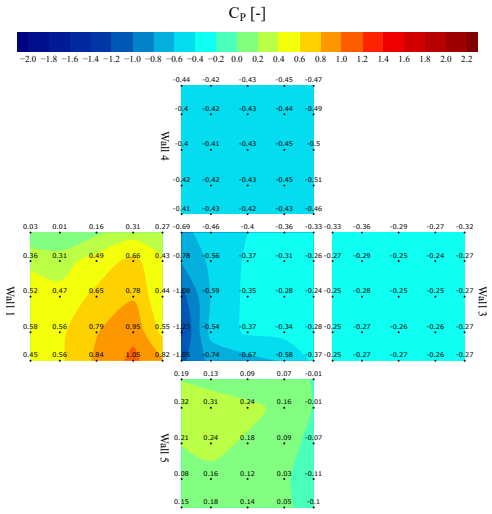

Figure 20: C_P contour maps at BDA tap coordinates, Realizable k-ϵ, 30°

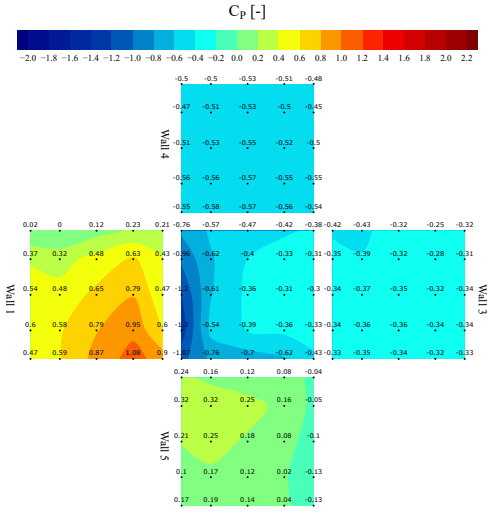

Figure 21: C_P contour maps at BDA tap coordinates, RNG k-ϵ, 30°

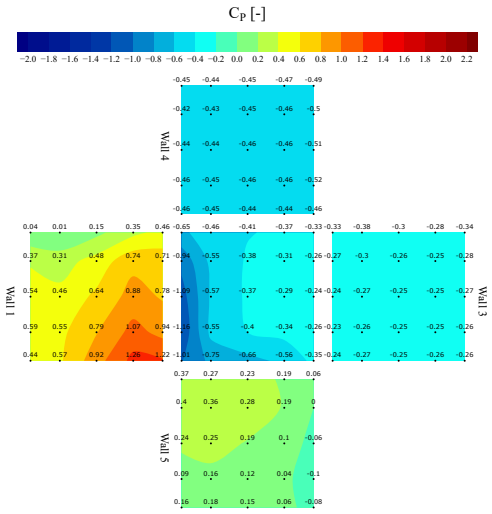

Figure 22: C_P contour maps at BDA tap coordinates, STD k-ω, 30°

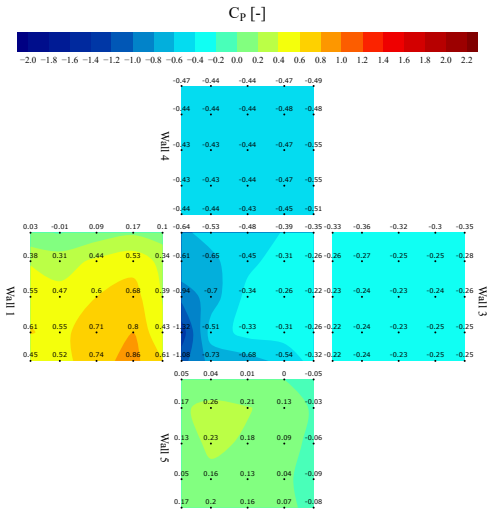

Figure 23: C_P contour maps at BDA tap coordinates, SST k-ω, 30°

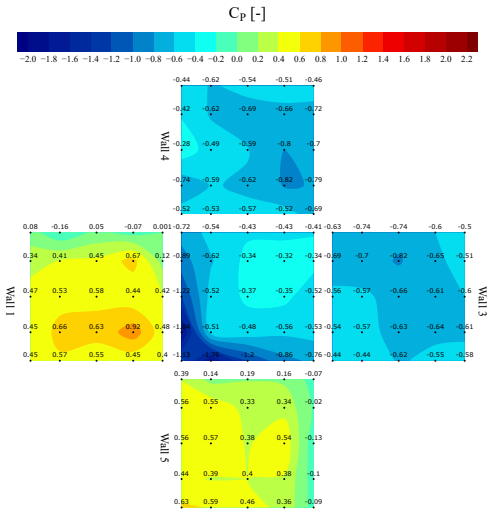

Figure 24: C_P contour maps, BDA 45°

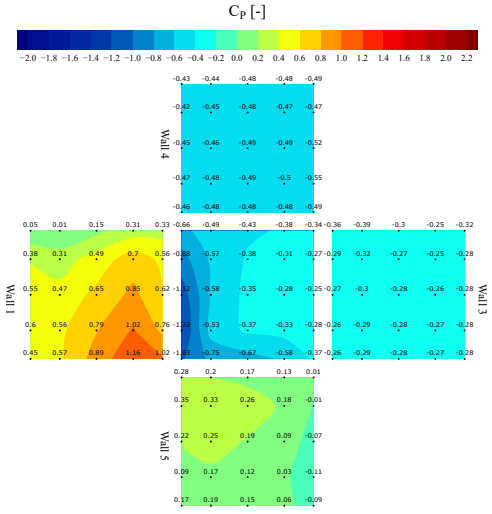

Figure 25: C_P contour maps at BDA tap coordinates, STD k-ϵ, 45°

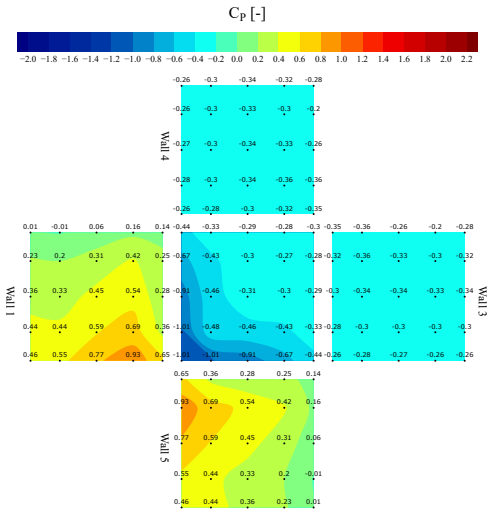

Figure 26: C_P contour maps at BDA tap coordinates, Realizable k-ϵ, 45°

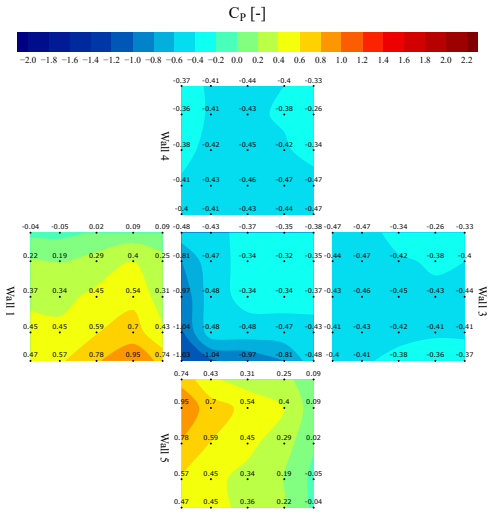

Figure 27: C_P contour maps at BDA tap coordinates, RNG k-ϵ, 45°

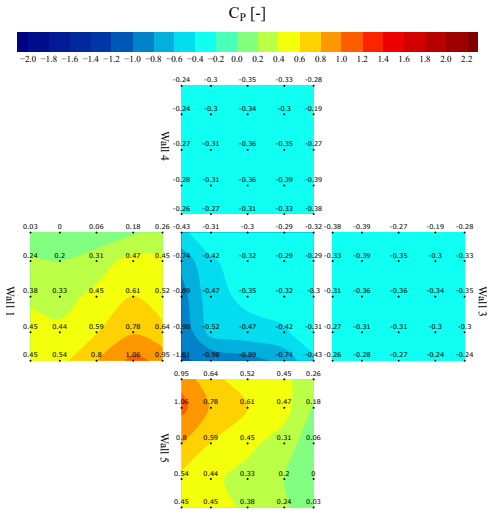

Figure 28: C_P contour maps at BDA tap coordinates, STD k-ω, 45°

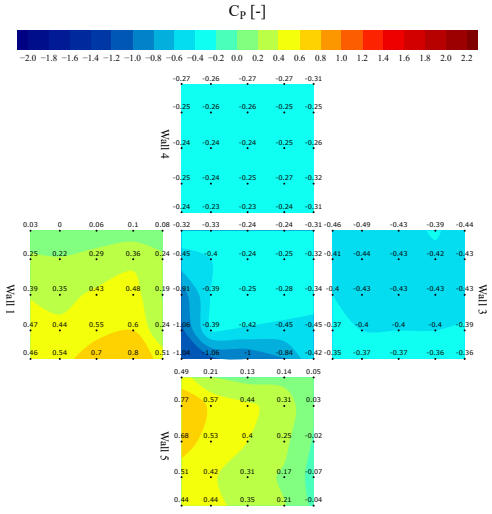

Figure 29: C_P contour maps at BDA tap coordinates, SST k-ω, 45°

2.2. Pressure Coefficient Contour Maps. TPU vs CFD

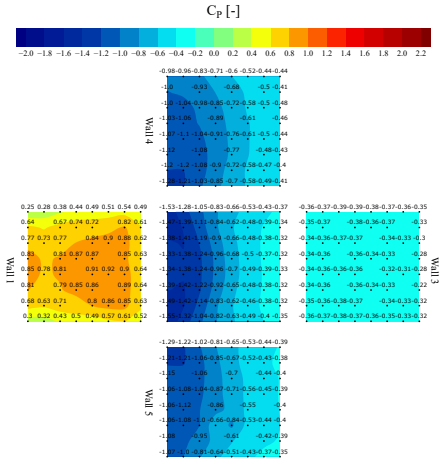

Figure 30: C_P contour maps, TPU 0°

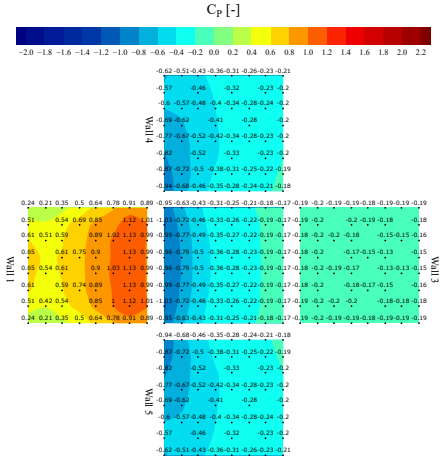

Figure 31: C_P contour maps at TPU tap coordinates, STD k-ϵ, 0°

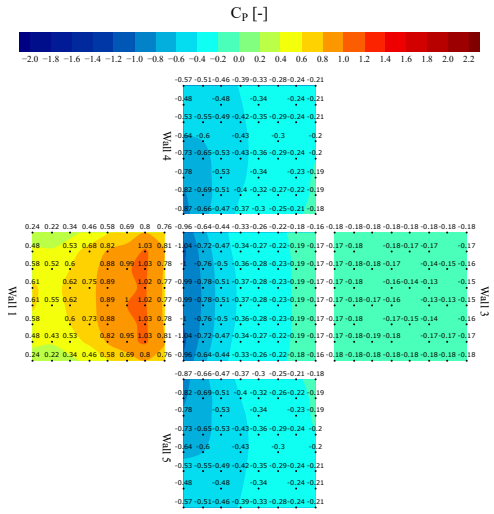

Figure 32: C_P contour maps at TPU tap coordinates, Realizable k-ϵ, 0°

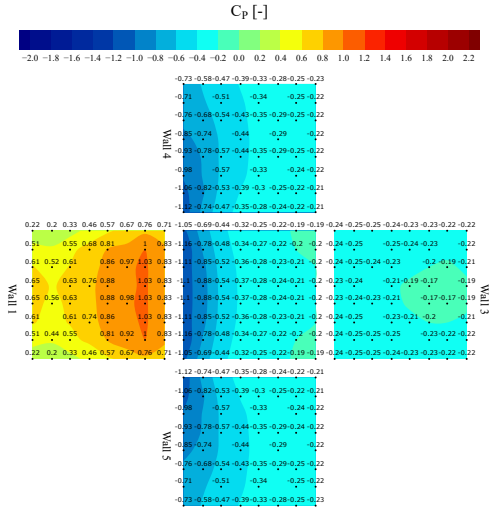

Figure 33: C_P contour maps at TPU tap coordinates, RNG k-ϵ, 0°

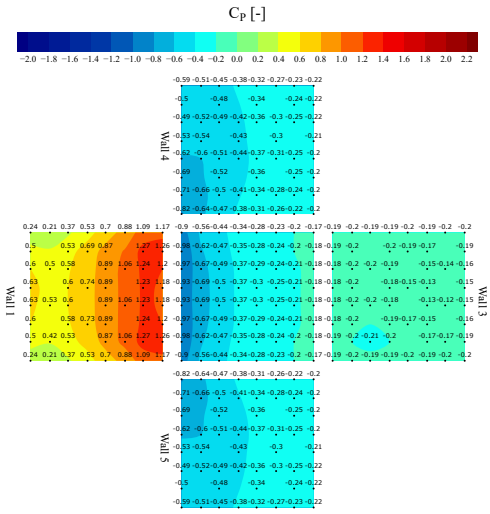

Figure 34: C_P contour maps at TPU tap coordinates, STD k-ω, 0°

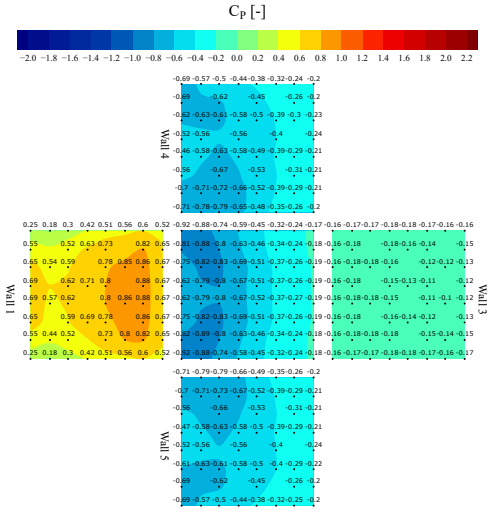

Figure 35: C_P contour maps at TPU tap coordinates, SST k-ω, 0°

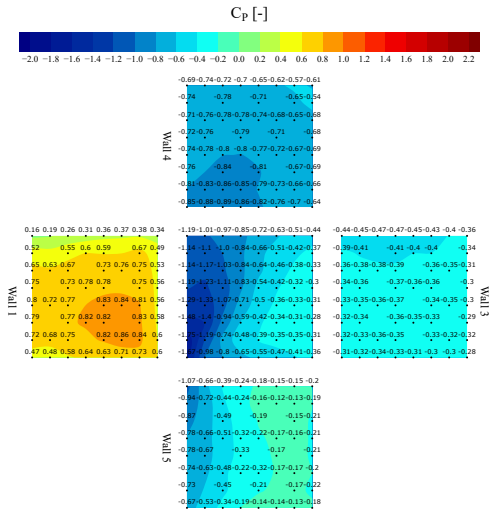

Figure 36: C_P contour maps, TPU 15°

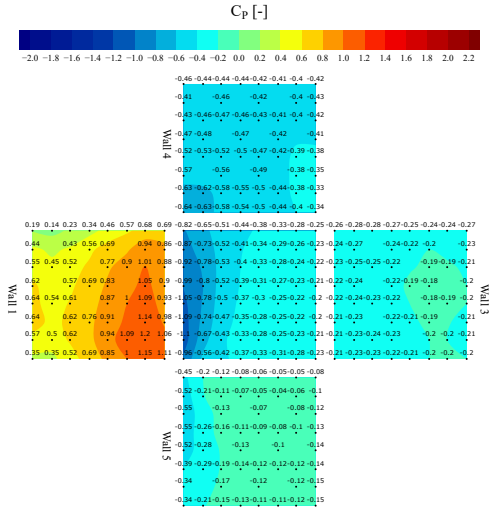

Figure 37: C_P contour maps at TPU tap coordinates, STD k-ϵ, 15°

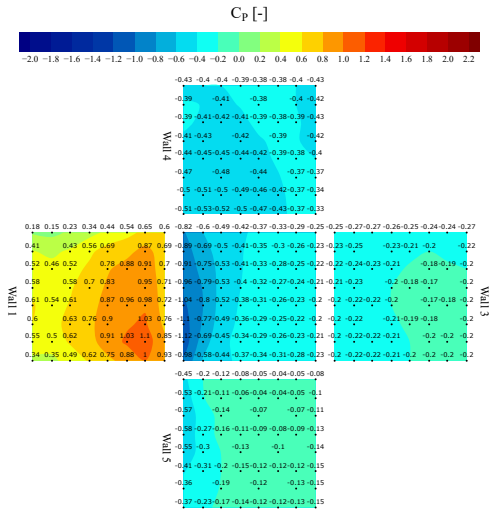

Figure 38: C_P contour maps at TPU tap coordinates, Realizable k-ϵ, 15°

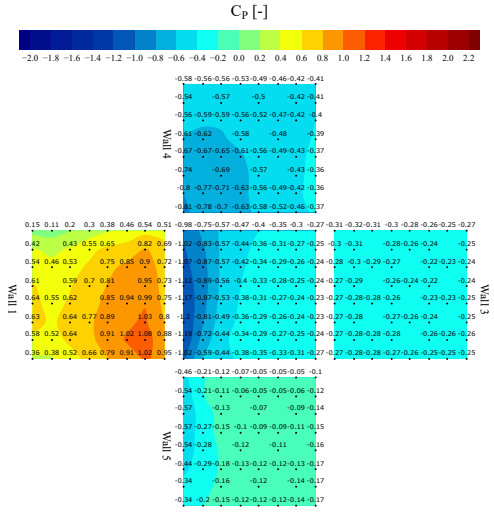

Figure 39: C_P contour maps at TPU tap coordinates, RNG k-ϵ, 15°

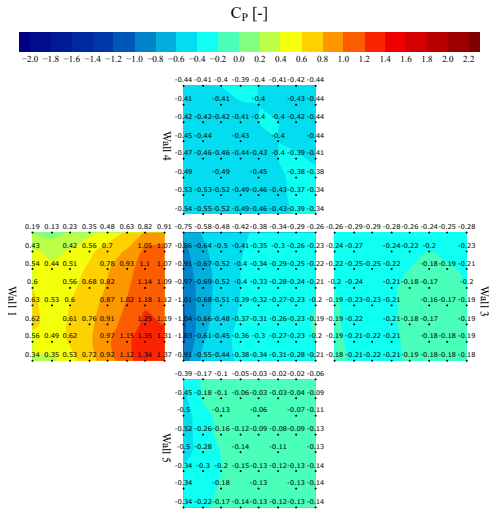

Figure 40: C_P contour maps at TPU tap coordinates, STD k-ω, 15°

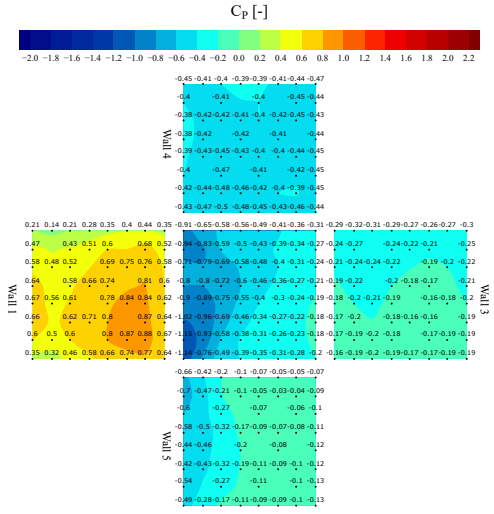

Figure 41: C_P contour maps at TPU tap coordinates, SST k-ω, 15°

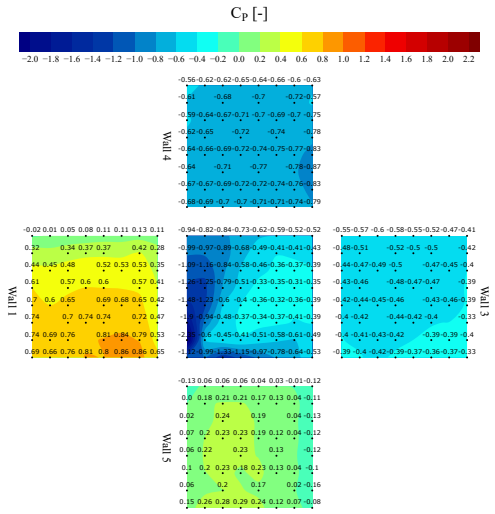

Figure 42: C_P contour maps, TPU 30°

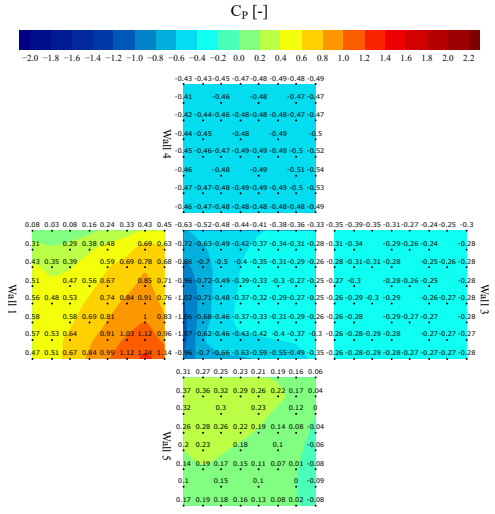

Figure 43: C_P contour maps at TPU tap coordinates, STD k-ϵ, 30°

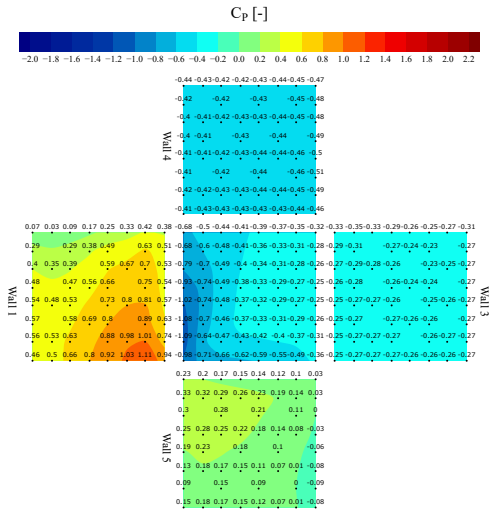

Figure 44: C_P contour maps at TPU tap coordinates, Realizable k-ϵ, 30°

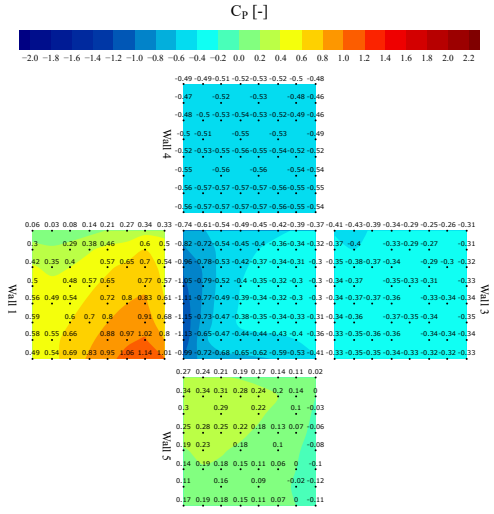

Figure 45: C_P contour maps at TPU tap coordinates, RNG k-ϵ, 30°

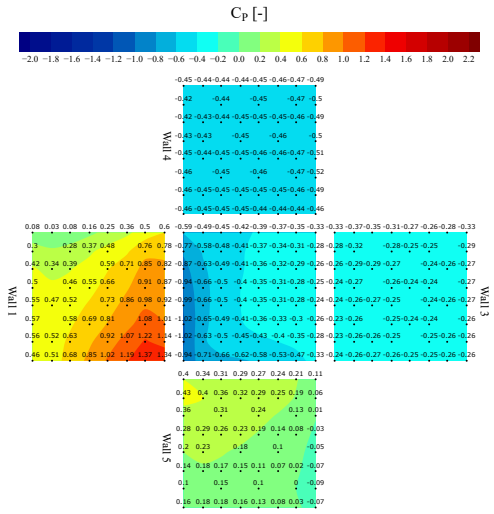

Figure 46: C_P contour maps at TPU tap coordinates, STD k-ω, 30°

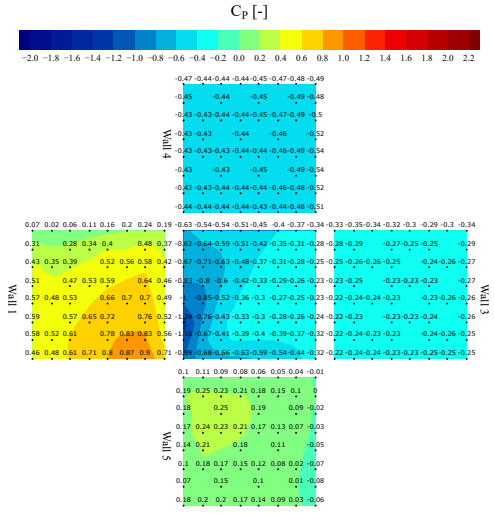

Figure 47: C_P contour maps at TPU tap coordinates, SST k-ω, 30°

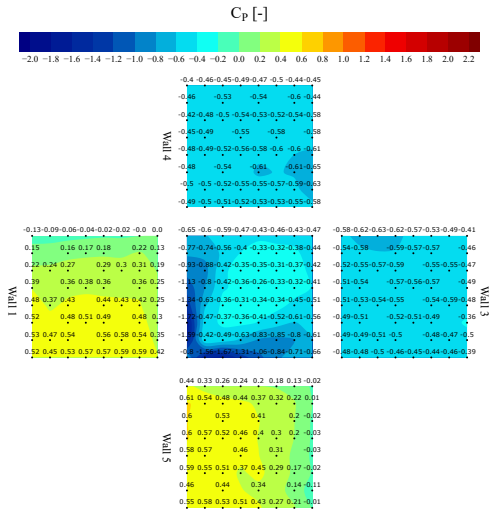

Figure 48: C_P contour maps, TPU 45°

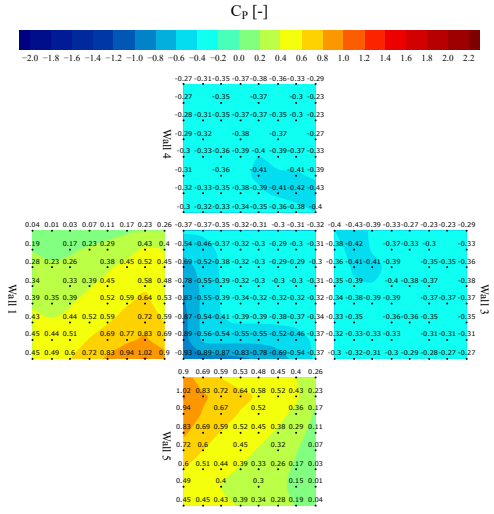

Figure 49: C_P contour maps at TPU tap coordinates, STD k-ϵ, 45°

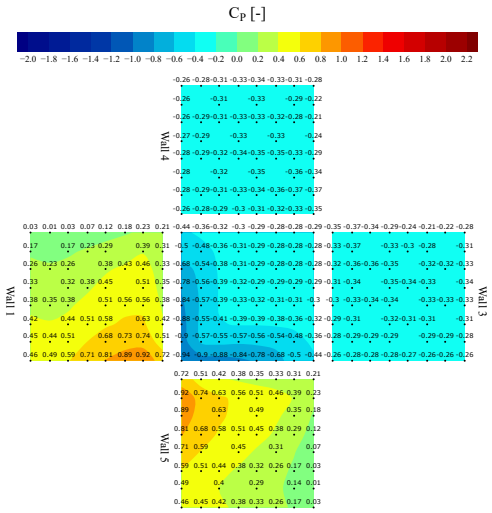

Figure 50: C_P contour maps at TPU tap coordinates, Realizable k-ϵ, 45°

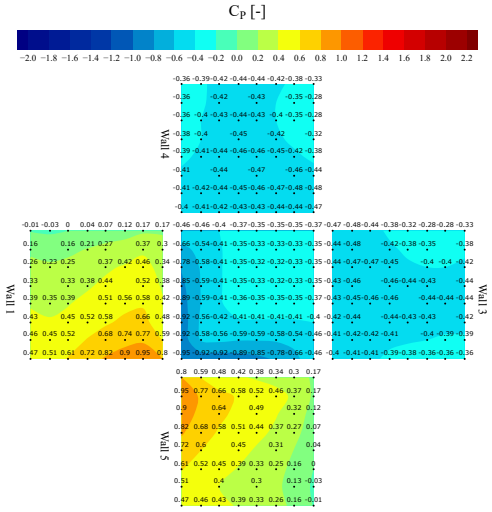

Figure 51: C_P contour maps at TPU tap coordinates, RNG k-ϵ, 45°

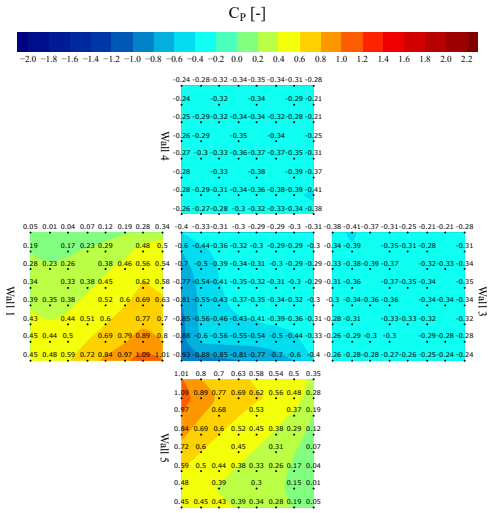

Figure 52: C_P contour maps at TPU tap coordinates, STD k-ω, 45°

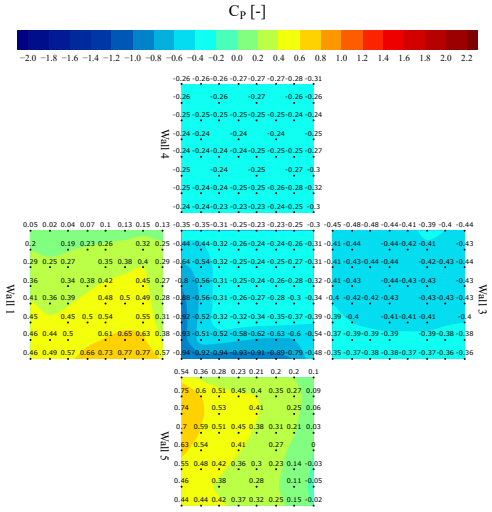

Figure 53: C_P contour maps at TPU tap coordinates, SST k-ω, 45°

2.3. *BDA and TPU Normalized Mean Square Error (NMSE) and Normalized Root Mean Square Error (ε)*

To assess the accuracy of the turbulence models against data from the BDA (Figure 56) and TPU (Figure 57) databases, the Normalized Mean Square Error (NMSE) and Normalized Root Mean Square Error (ε) were computed for each wall and for all turbulence models (see Equations (2) and (3)). NMSE quantifies the model's overall performance across the dataset. According to stringent validation criteria, an NMSE of zero indicates perfect agreement, while values below 1.5 are considered acceptable for accurate simulations. NMSE is defined as:

$$NMSE = \frac{\sum_{i=1}^{n}(y_i - \hat{y})^2}{\sum_{i=1}^{n} y_i \ \hat{y}} \tag{2}$$

Similarly, the normalized root mean square error (ε) is given by:

$$\varepsilon = \frac{\sqrt{\frac{\sum_{i=1}^{n}(y_i - \hat{y})^2}{n}}}{\overline{y}} \tag{3}$$

where y_i and $\hat{y}$ are the observed and predicted C_P values at the ith tap position, respectively, n is the total number of taps on the wall, and $\overline{y}$ is the mean wall C_P value.

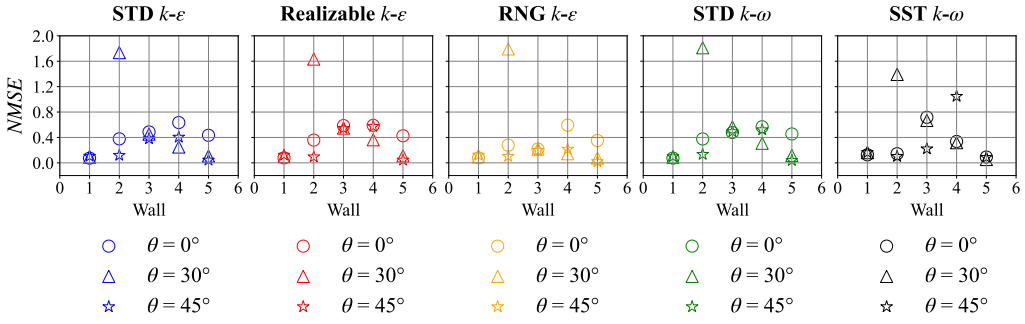

Figure 54: $NMSE$ refered to BDA basedata per wall for all turbulence models.

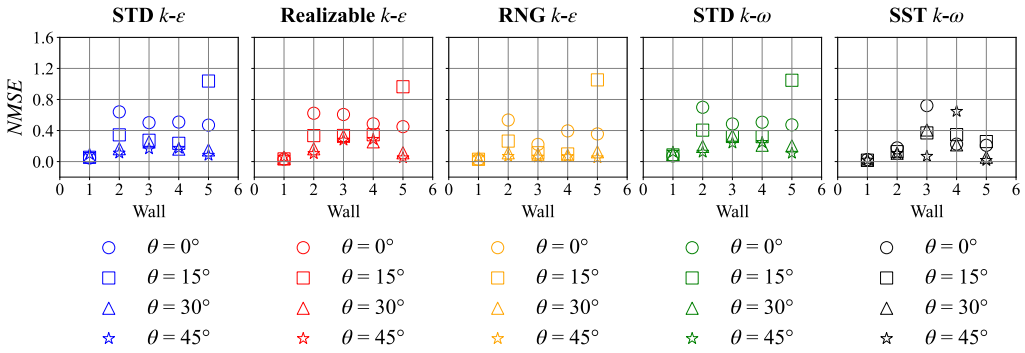

Figure 55: $NMSE$ refered to TPU basedata per wall for all turbulence models.

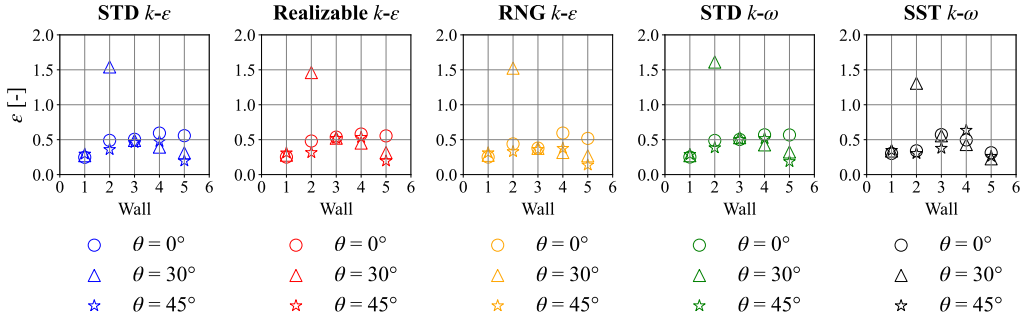

Figure 56: ε refered to BDA basedata per wall for all turbulence models.

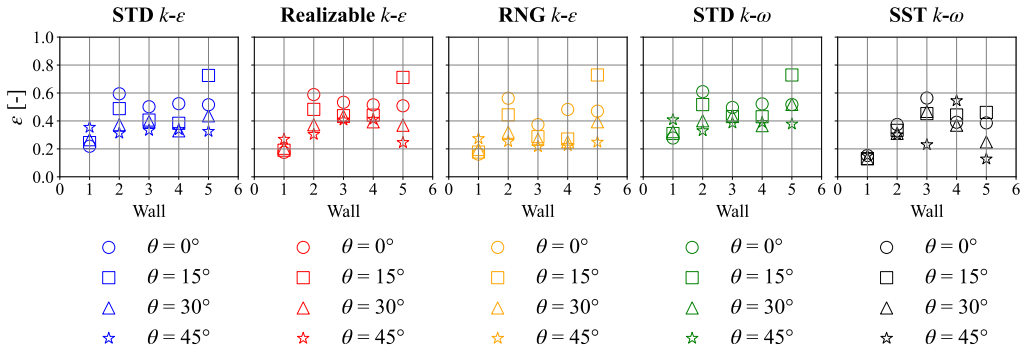

Figure 57: ε refered to TPU basedata per wall for all turbulence models.

2.4. Comparison Of Pressure Coefficients At Wall Center-lines With Respect To Databases

Figure 58 illustrates the relative positions of the pressure taps in the BDA and TPU experimental studies. For clarity, the blue line will henceforth be referred to as the "horizontal center-line", and the red line as the "vertical center-line".

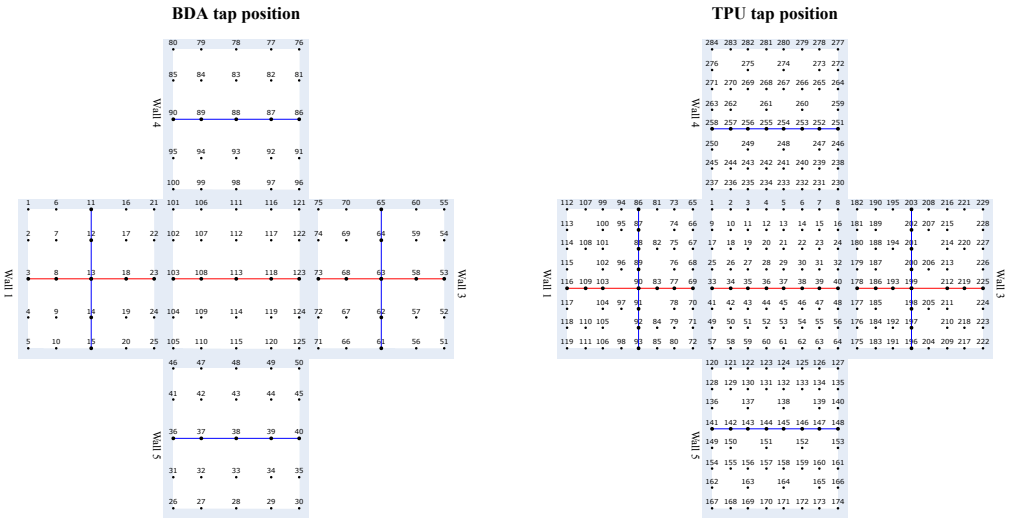

(a) BDA center-lines

(b) TPU center-lines

Figure 58: Center-lines at BDA and TPU tap position

Figures 59 to 62 present the local pressure coefficients along the horizontal and vertical center-lines for wind incidence angles of 0°, 15°, 30°, and 45°. These results are compared with experimental data obtained from the BDA and TPU datasets.

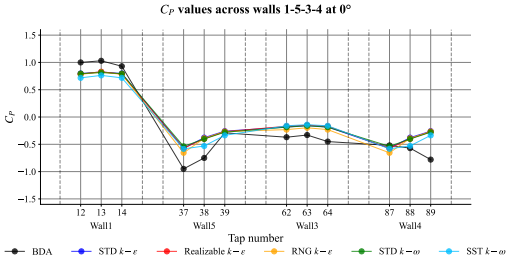

(a) BDA C_P at horizontal center-line at 0°

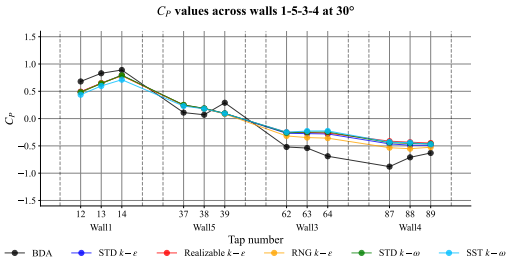

(b) BDA C_P at horizontal center-line at 30°

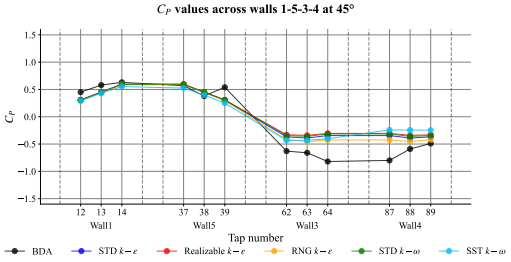

(c) BDA C_P at horizontal center-line at 45°

Figure 59: BDA C_P along horizontal center-line

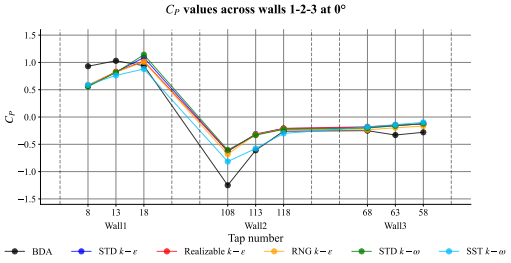

(a) BDA C_P at vertical center-line at 0°

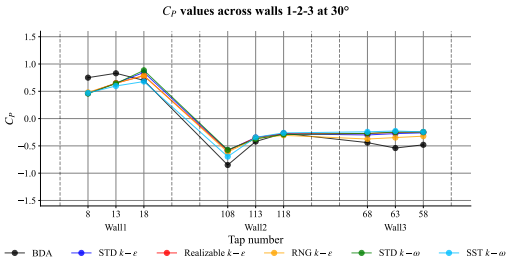

(b) BDA C_P at vertical center-line at 30°

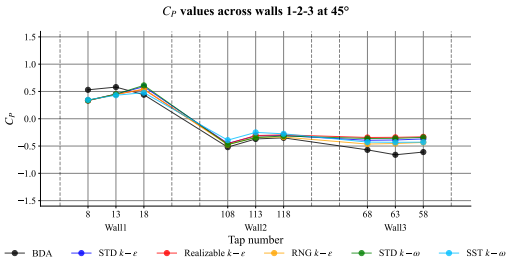

(c) BDA C_P at vertical center-line at 45°

Figure 60: BDA C_P along vertical center-line

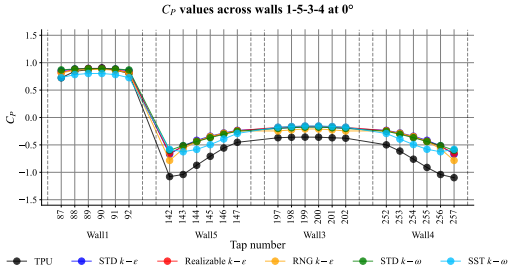

(a) TPU C_P at horizontal center-line at 0°

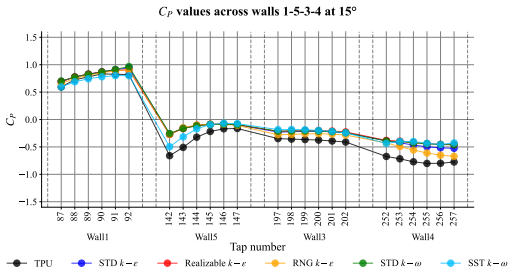

(b) TPU C_P at horizontal center-line at 15°

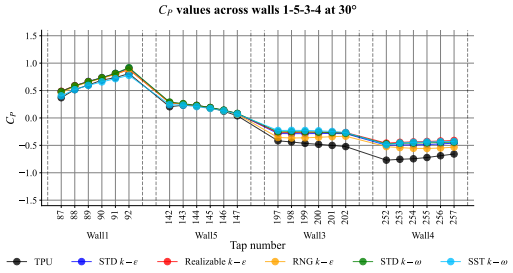

(c) TPU C_P at horizontal center-line at 30°

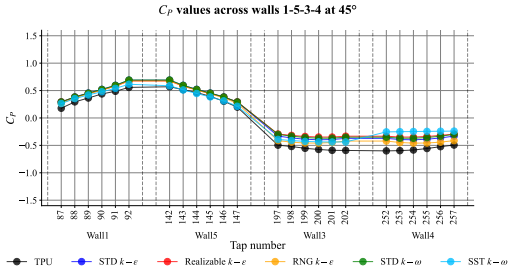

(d) TPU C_P at horizontal center-line at 45°

Figure 61: TPU C_P along horizontal center-line

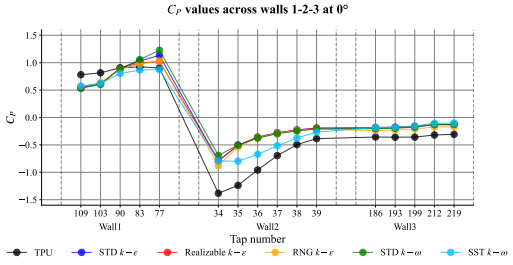

(a) TPU C_P at vertical center-line at 0°

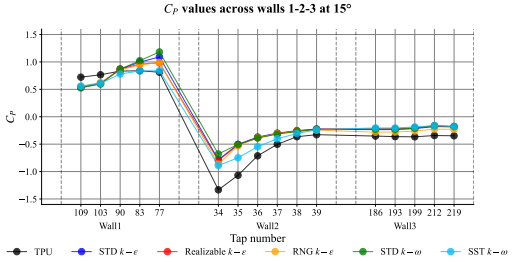

(b) TPU C_P at vertical center-line at 15°

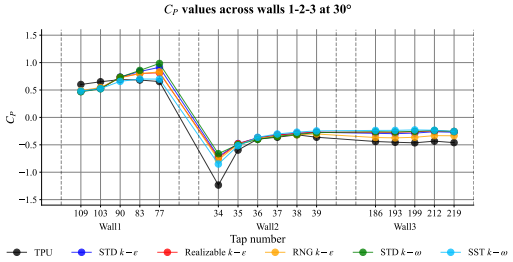

(c) TPU C_P at vertical center-line at 30°

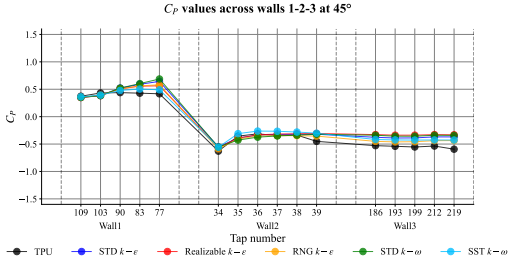

(d) TPU C_P at vertical center-line at 45°

Figure 62: TPU C_P along vertical center-line

2.5. *Turbulent Kinetic Energy and Turbulent Viscosity Fields in Parallel and Cross-Sectional Planes*

Figures 64 to 78 present H/2 sections, oriented parallel and transverse to the flow, illustrating the turbulent viscosity variable for the studied turbulence models at wind incidence angles of 0°, 15°, 30°, and 45°.

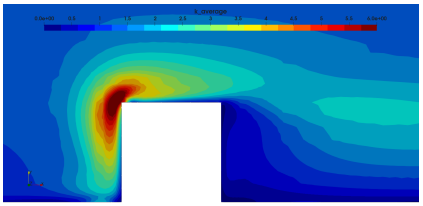

(a) Turbulent kinetic energy (k) field in the parallel flow plane for the STD k-ϵ model at 0°

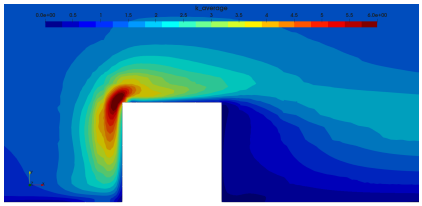

(b) Turbulent kinetic energy (k) field in the parallel flow plane for the Realizable k-ϵ model at 0°

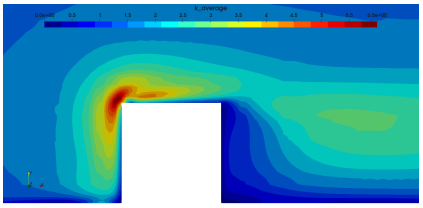

(c) Turbulent kinetic energy (k) field in the parallel flow plane for the RNG k-ϵ model at 0°

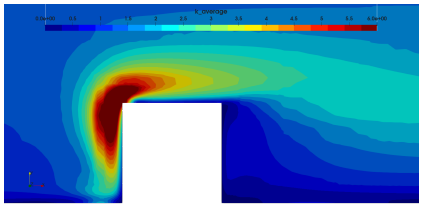

(d) Turbulent kinetic energy (k) field in the parallel flow plane for the STD k-ω model at 0°

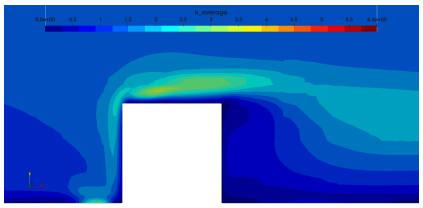

(e) Turbulent kinetic energy (k) field in the parallel flow plane for the SST k-ω model at 0°

Figure 63: Turbulent kinetic energy (k) field in the parallel flow plane for tested turbulence models at 0°

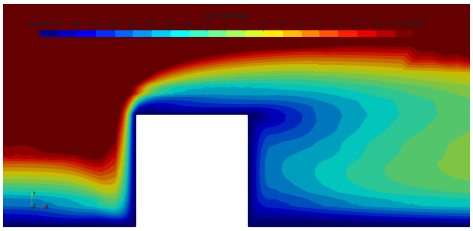

(a) Turbulent viscosity (ν_t) field in the parallel flow plane for the STD k-ϵ model at 0°

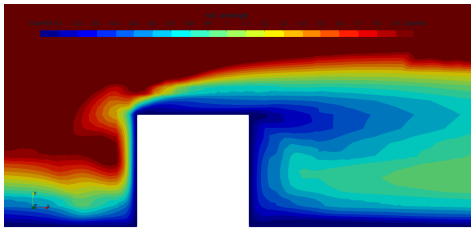

(b) Turbulent viscosity (ν_t) field in the parallel flow plane for the Realizable k-ϵ model at 0°

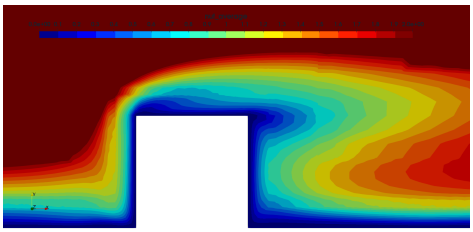

(c) Turbulent viscosity (ν_t) field in the parallel flow plane for the RNG k-ϵ model at 0°

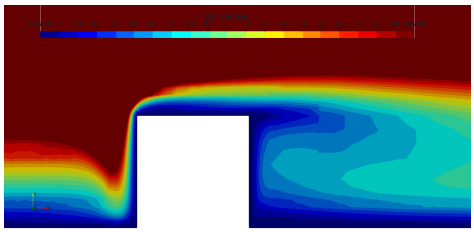

(d) Turbulent viscosity (ν_t) field in the parallel flow plane for the STD k-ω model at 0°

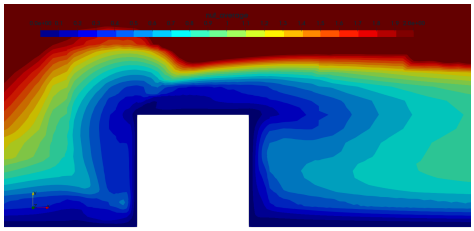

(e) Turbulent viscosity (ν_t) field in the parallel flow plane for the SST k-ω model at 0°

Figure 64: Turbulent viscosity (ν_t) field in the parallel flow plane for tested turbulence models at 0°

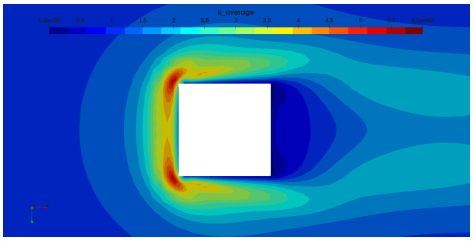

(a) Turbulent kinetic energy (k) field in the cross-sectional plane for the STD k-ϵ model at 0°

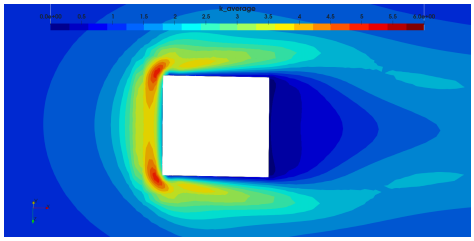

(b) Turbulent kinetic energy (k) field in the cross-sectional plane for the Realizable k-ϵ model at 0°

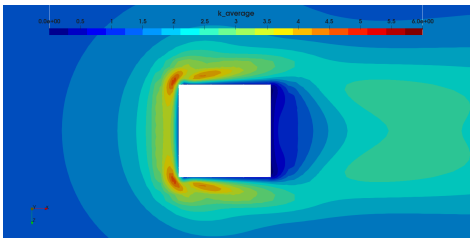

(c) Turbulent kinetic energy (k) field in the cross-sectional plane for the RNG k-ϵ model at 0°

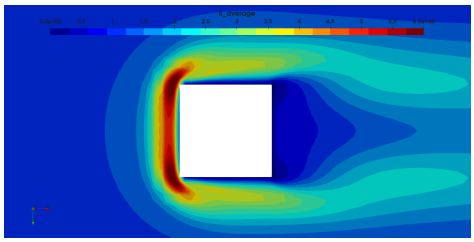

(d) Turbulent kinetic energy (k) field in the cross-sectional plane for the STD k-ω model at 0°

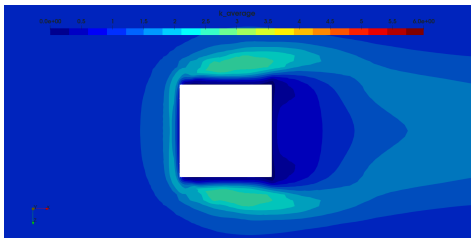

(e) Turbulent kinetic energy (k) field in the cross-sectional plane for the SST k-ω model at 0°

Figure 65: Cross-sectional turbulent kinetic energy (k) field for tested turbulence models at 0°

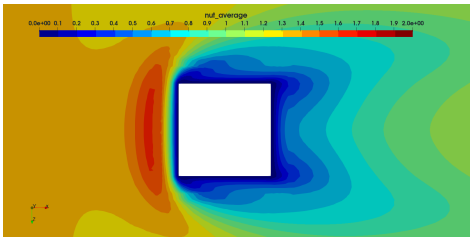

(a) Turbulent viscosity (ν_t) field in the cross-sectional plane for the STD k-ϵ model at 0°

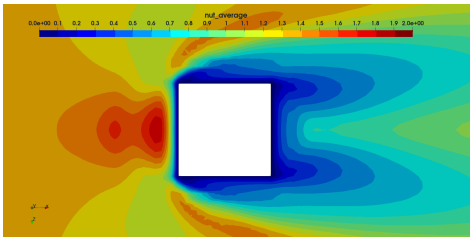

(b) Turbulent viscosity (ν_t) field in the cross-sectional plane for the Real k-ϵ model at 0°

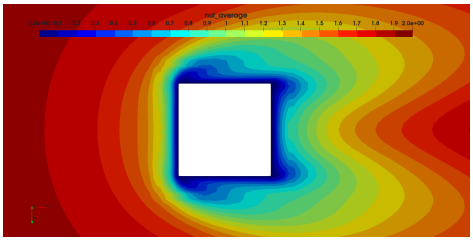

(c) Turbulent viscosity (ν_t) field in the cross-sectional plane for the RNG k-ϵ model at 0°

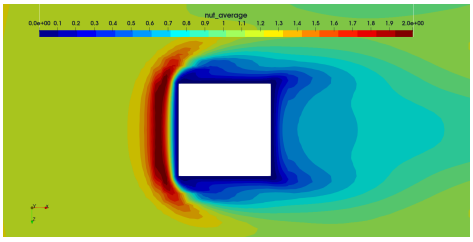

(d) Turbulent viscosity (ν_t) field in the cross-sectional plane for the STD k-ω model at 0°

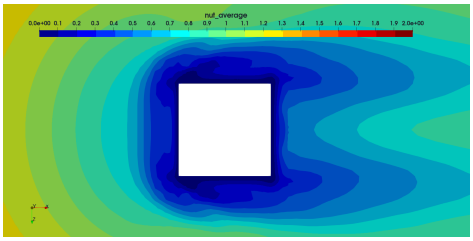

(e) Turbulent viscosity (ν_t) field in the cross-sectional plane for the SST k-ω model at 0°

Figure 66: Cross-sectional turbulent viscosity (ν_t) field for tested turbulence models at 0°

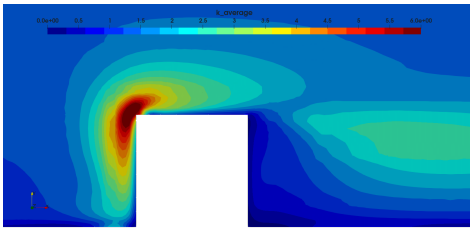

(a) Turbulent kinetic energy (k) field in the parallel flow plane for the STD k-ϵ model at 15°

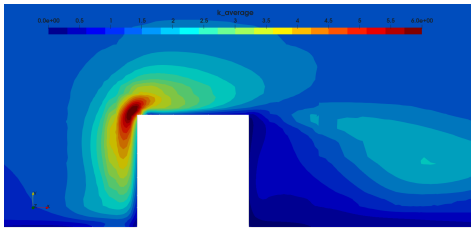

(b) Turbulent kinetic energy (k) field in the parallel flow plane for the Real k-ϵ model at 15°

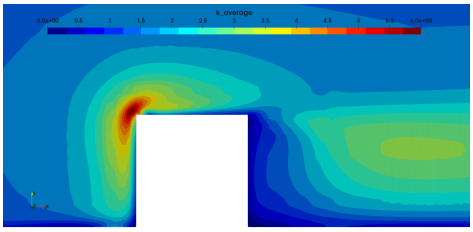

(c) Turbulent kinetic energy (k) field in the parallel flow plane for the RNG k-ϵ model at 15°

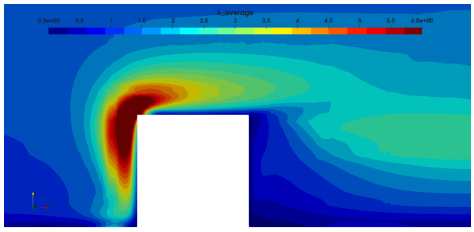

(d) Turbulent kinetic energy (k) field in the parallel flow plane for the STD k-ω model at 15°

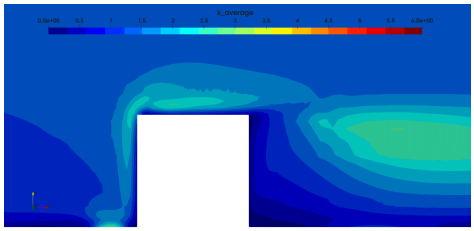

(e) Turbulent kinetic energy (k) field in the parallel flow plane for the SST k-ω model at 15°

Figure 67: Turbulent kinetic energy (k) field in the parallel flow plane for tested turbulence models at 15°

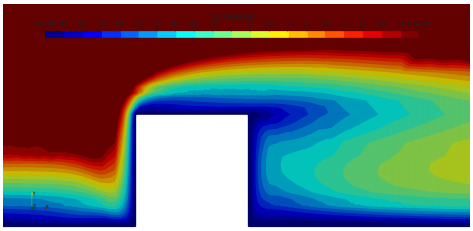

(a) Turbulent viscosity (ν_t) field in the parallel flow plane for the STD k-ϵ model at 15°

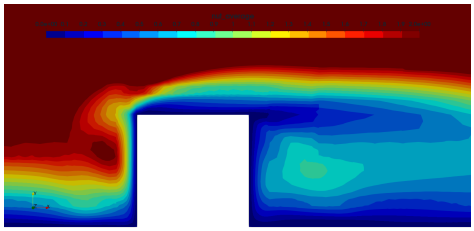

(b) Turbulent viscosity (ν_t) field in the parallel flow plane for the Realizable k-ϵ model at 15°

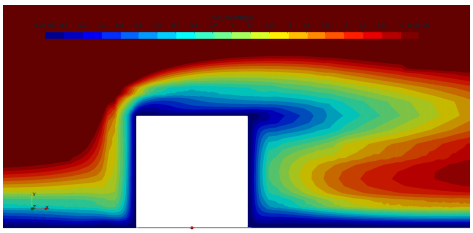

(c) Turbulent viscosity (ν_t) field in the parallel flow plane for the RNG k-ϵ model at 15°

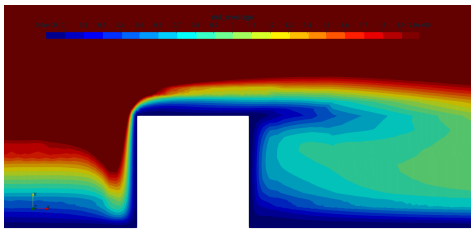

(d) Turbulent viscosity (ν_t) field in the parallel flow plane for the STD k-ω model at 15°

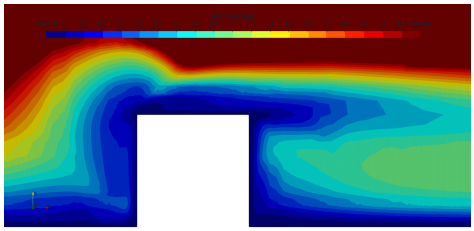

(e) Turbulent viscosity (ν_t) field in the parallel flow plane for the SST k-ω model at 15°

Figure 68: Turbulent viscosity (ν_t) field in the parallel flow plane for tested turbulence models at 15°

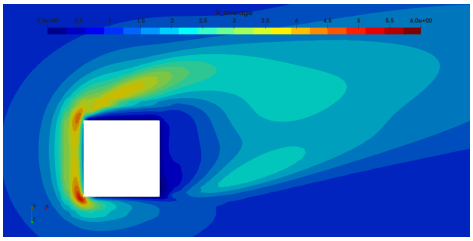

(a) Turbulent kinetic energy (k) field in the cross-sectional plane for the STD k-ϵ model at 15°

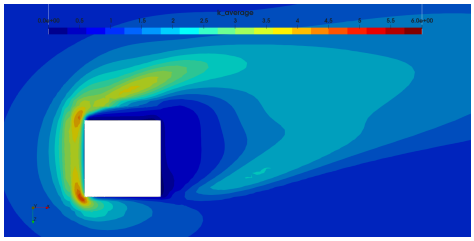

(b) Turbulent kinetic energy (k) field in the cross-sectional plane for the Realizable k-ϵ model at 15°

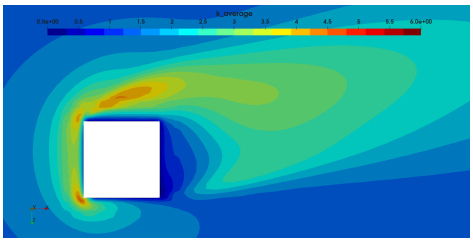

(c) Turbulent kinetic energy (k) field in the cross-sectional plane for the RNG k-ϵ model at 15°

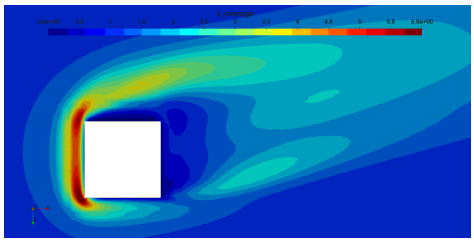

(d) Turbulent kinetic energy (k) field in the cross-sectional plane for the STD k-ω model at 15°

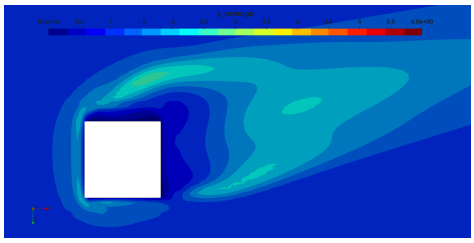

(e) Turbulent kinetic energy (k) field in the cross-sectional plane for the SST k-ω model at 15°

Figure 69: Cross-sectional turbulent kinetic energy (k) field for tested turbulence models at 15°

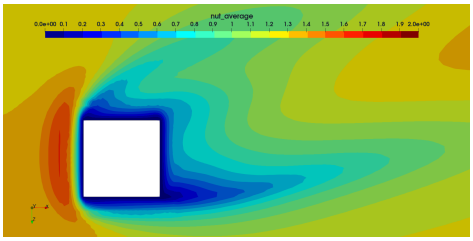

(a) Turbulent viscosity (ν_t) field in the cross-sectional plane for the STD k-ϵ model at 15°

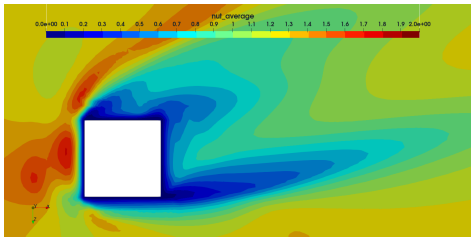

(b) Turbulent viscosity (ν_t) field in the cross-sectional plane for the Real k-ϵ model at 15°

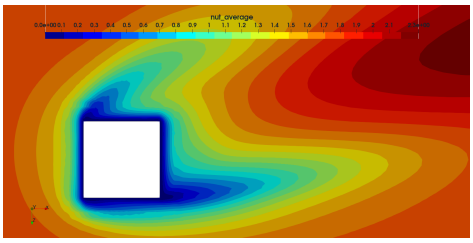

(c) Turbulent viscosity (ν_t) field in the cross-sectional plane for the RNG k-ϵ model at 15°

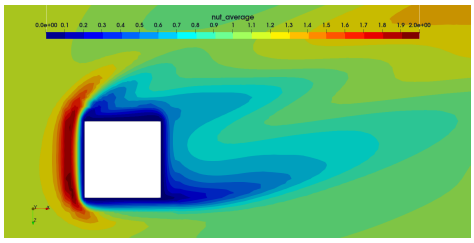

(d) Turbulent viscosity (ν_t) field in the cross-sectional plane for the STD k-ω model at 15°

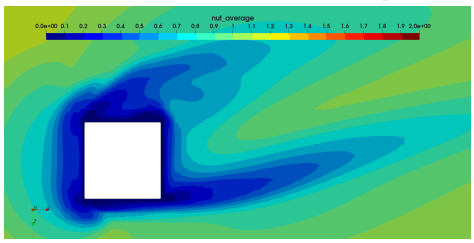

(e) Turbulent viscosity (ν_t) field in the cross-sectional plane for the SST k-ω model at 15°

Figure 70: Cross-sectional turbulent viscosity (ν_t) field for tested turbulence models at 15°

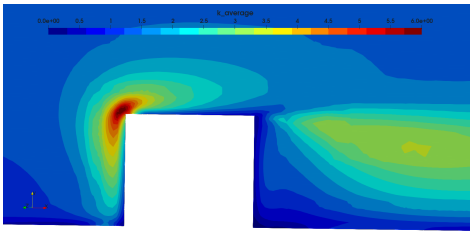

(a) Turbulent kinetic energy (k) field in the parallel flow plane for the STD k-ϵ model at 30°

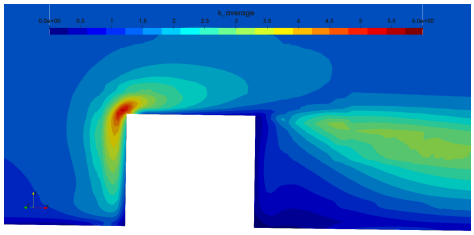

(b) Turbulent kinetic energy (k) field in the parallel flow plane for the Real k-ϵ model at 30°

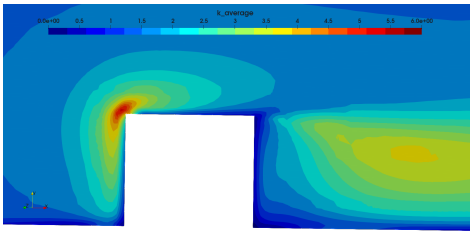

(c) Turbulent kinetic energy (k) field in the parallel flow plane for the RNG k-ϵ model at 30°

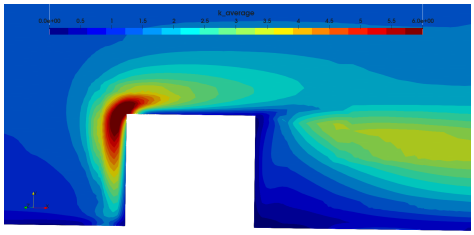

(d) Turbulent kinetic energy (k) field in the parallel flow plane for the STD k-ω model at 30°

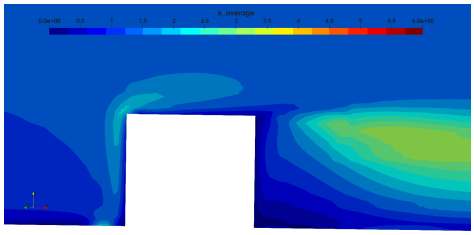

(e) Turbulent kinetic energy (k) field in the parallel flow plane for the SST k-ω model at 30°

Figure 71: Turbulent kinetic energy (k) field in the parallel flow plane for tested turbulence models at 30°

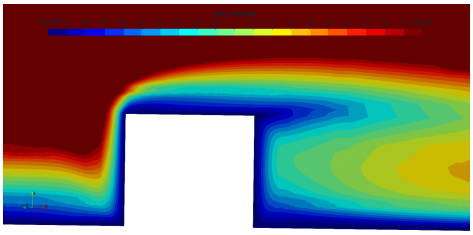

(a) Turbulent viscosity (ν_t) field in the parallel flow plane for the STD k-ϵ model at 30°

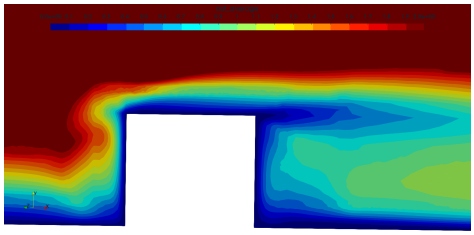

(b) Turbulent viscosity (ν_t) field in the parallel flow plane for the Realizable k-ϵ model at 30°

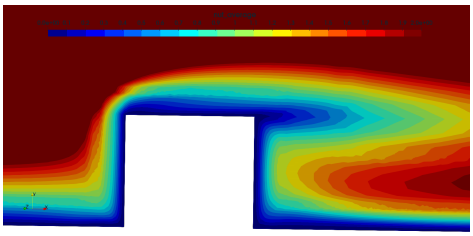

(c) Turbulent viscosity (ν_t) field in the parallel flow plane for the RNG k-ϵ model at 30°

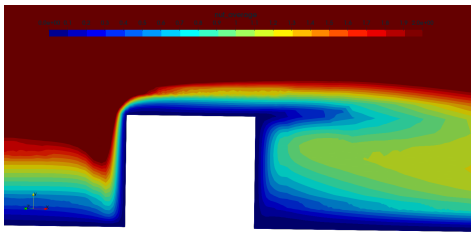

(d) Turbulent viscosity (ν_t) field in the parallel flow plane for the STD k-ω model at 30°

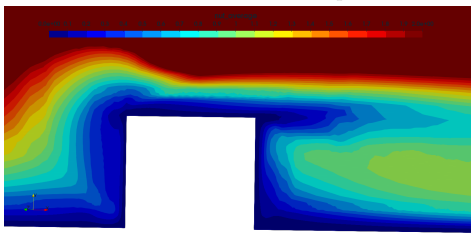

(e) Turbulent viscosity (ν_t) field in the parallel flow plane for the SST k-ω model at 30°

Figure 72: Turbulent viscosity (ν_t) field in the parallel flow plane for tested turbulence models at 30°

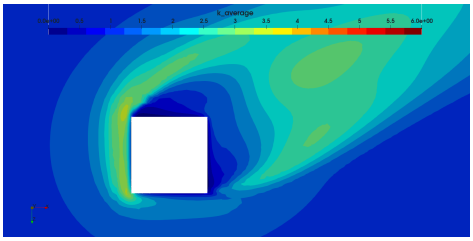

(a) Turbulent kinetic energy (k) field in the cross-sectional plane for the STD k-ϵ model at 30°

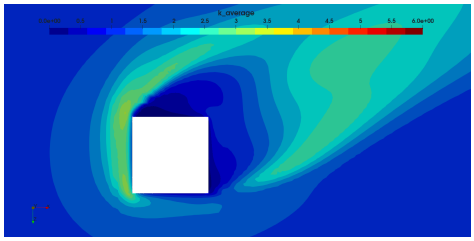

(b) Turbulent kinetic energy (k) field in the cross-sectional plane for the Realizable k-ϵ model at 30°

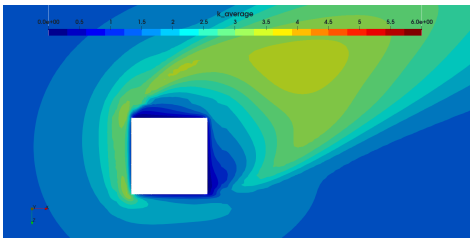

(c) Turbulent kinetic energy (k) field in the cross-sectional plane for the RNG k-ϵ model at 30°

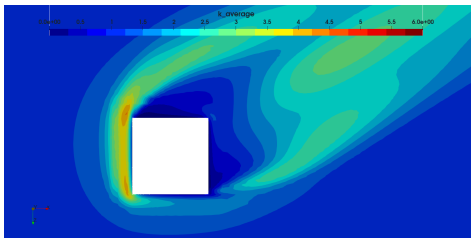

(d) Turbulent kinetic energy (k) field in the cross-sectional plane for the STD k-ω model at 30°

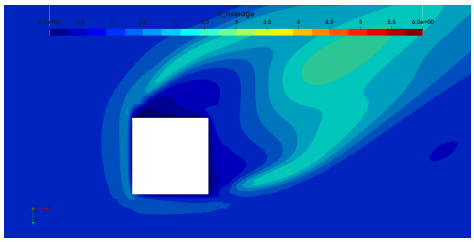

(e) Turbulent kinetic energy (k) field in the cross-sectional plane for the SST k-ω model at 30°

Figure 73: Cross-sectional turbulent kinetic energy (k) field for tested turbulence models at 30°

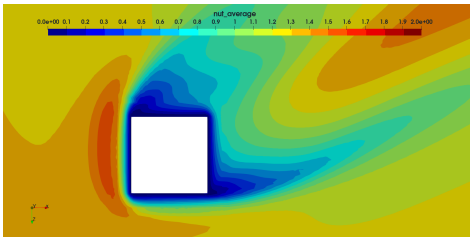

(a) Turbulent viscosity (ν_t) field in the cross-sectional plane for the STD k-ϵ model at 30°

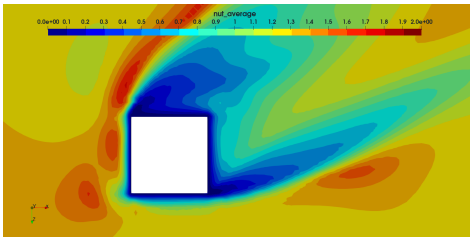

(b) Turbulent viscosity (ν_t) field in the cross-sectional plane for the Real k-ϵ model at 30°

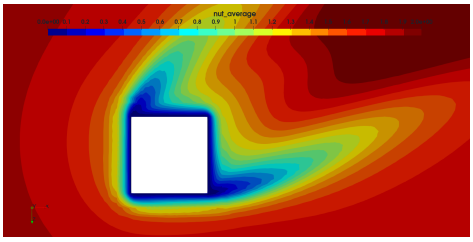

(c) Turbulent viscosity (ν_t) field in the cross-sectional plane for the RNG k-ϵ model at 30°

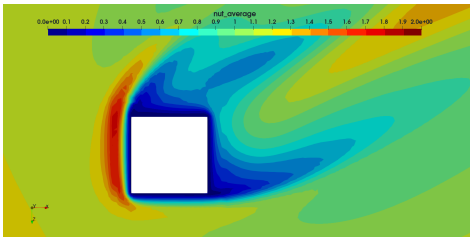

(d) Turbulent viscosity (ν_t) field in the cross-sectional plane for the STD k-ω model at 30°

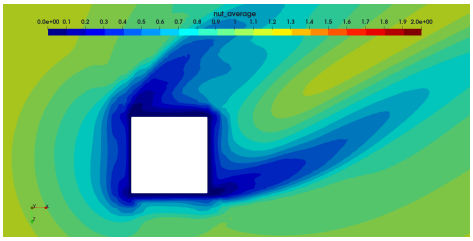

(e) Turbulent viscosity (ν_t) field in the cross-sectional plane for the SST k-ω model at 30°

Figure 74: Cross-sectional turbulent viscosity (ν_t) field for tested turbulence models at 30°

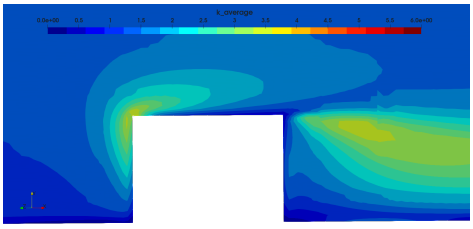

(a) Turbulent kinetic energy (k) field in the parallel flow plane for the STD k-ϵ model at 45°

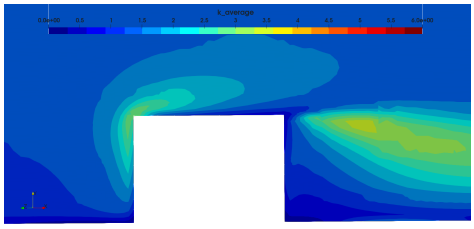

(b) Turbulent kinetic energy (k) field in the parallel flow plane for the Real k-ϵ model at 45°

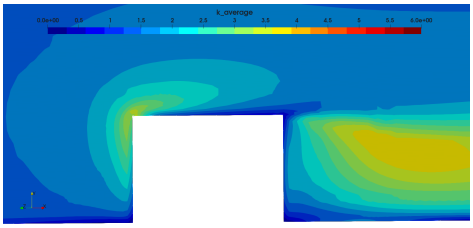

(c) Turbulent kinetic energy (k) field in the parallel flow plane for the RNG k-ϵ model at 45°

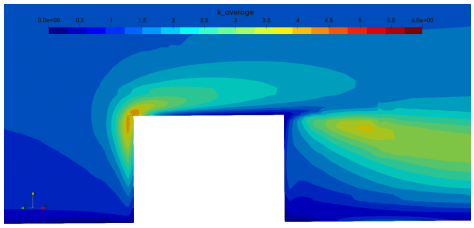

(d) Turbulent kinetic energy (k) field in the parallel flow plane for the STD k-ω model at 45°

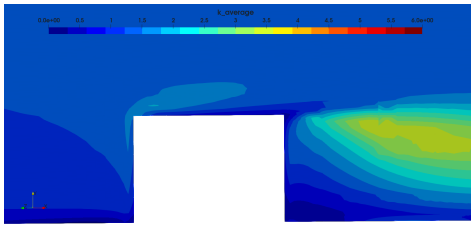

(e) Turbulent kinetic energy (k) field in the parallel flow plane for the SST k-ω model at 45°

Figure 75: Turbulent kinetic energy (k) field in the parallel flow plane for tested turbulence models at 45°

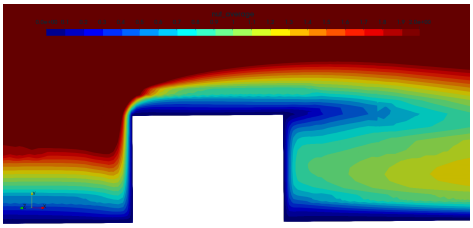

(a) Turbulent viscosity (ν_t) field in the parallel flow plane for the STD k-ϵ model at 45°

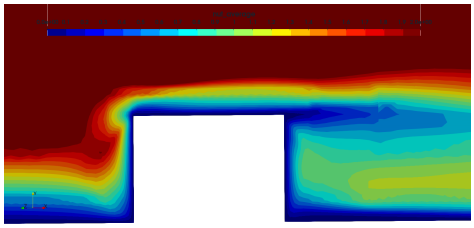

(b) Turbulent viscosity (ν_t) field in the parallel flow plane for the Realizable k-ϵ model at 45°

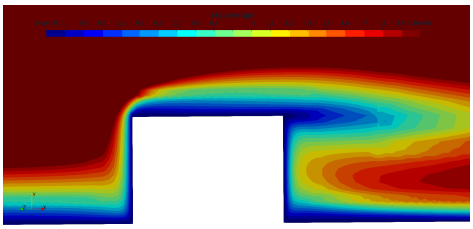

(c) Turbulent viscosity (ν_t) field in the parallel flow plane for the RNG k-ϵ model at 45°

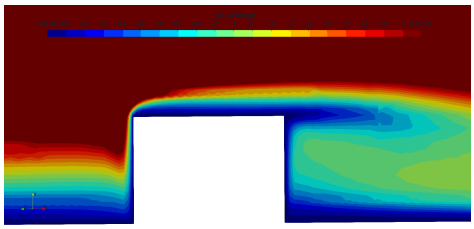

(d) Turbulent viscosity (ν_t) field in the parallel flow plane for the STD k-ω model at 45°

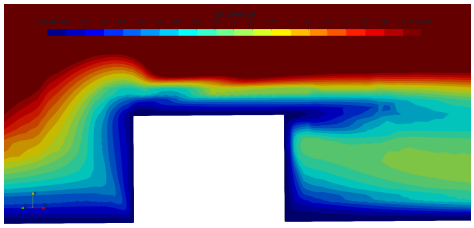

(e) Turbulent viscosity (ν_t) field in the parallel flow plane for the SST k-ω model at 45°

Figure 76: Turbulent viscosity (ν_t) field in the parallel flow plane for tested turbulence models at 45°

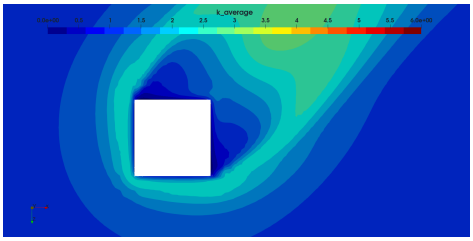

(a) Turbulent kinetic energy (k) field in the cross-sectional plane for the STD k-ϵ model at 45°

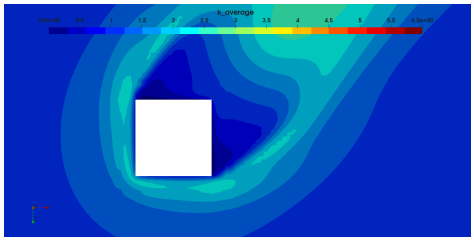

(b) Turbulent kinetic energy (k) field in the cross-sectional plane for the Realizable k-ϵ model at 45°

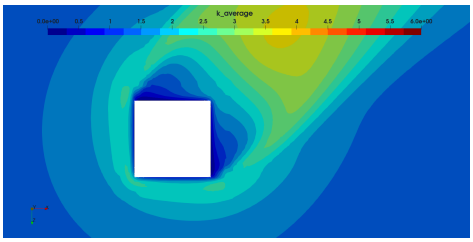

(c) Turbulent kinetic energy (k) field in the cross-sectional plane for the RNG k-ϵ model at 45°

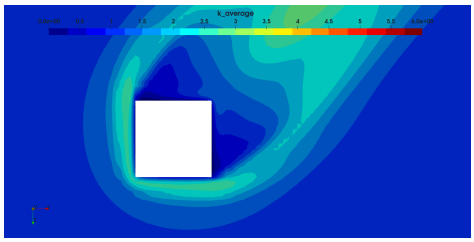

(d) Turbulent kinetic energy (k) field in the cross-sectional plane for the STD k-ω model at 45°

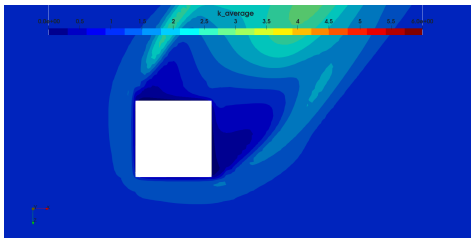

(e) Turbulent kinetic energy (k) field in the cross-sectional plane for the SST k-ω model at 45°

Figure 77: Cross-sectional turbulent kinetic energy (k) field for tested turbulence models at 45°

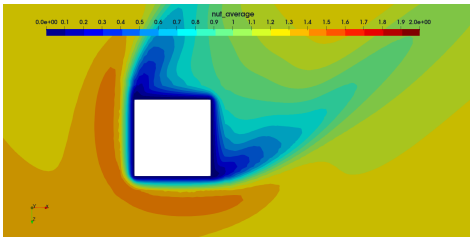

(a) Turbulent viscosity (ν_t) field in the cross-sectional plane for the STD k-ϵ model at 45°

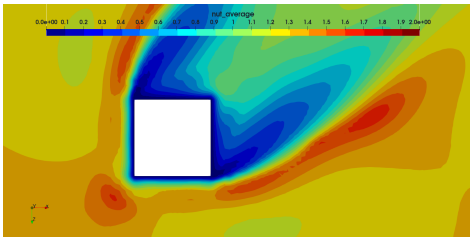

(b) Turbulent viscosity (ν_t) field in the cross-sectional plane for the Real k-ϵ model at 45°

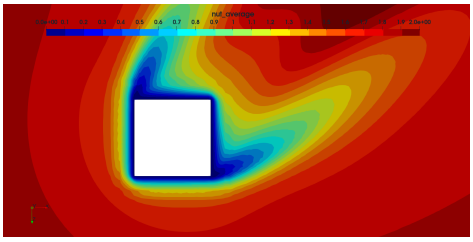

(c) Turbulent viscosity (ν_t) field in the cross-sectional plane for the RNG k-ϵ model at 45°

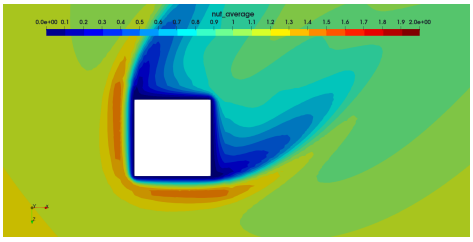

(d) Turbulent viscosity (ν_t) field in the cross-sectional plane for the STD k-ω model at 45°

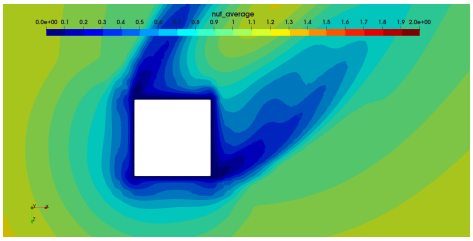

(e) Turbulent viscosity (ν_t) field in the cross-sectional plane for the SST k-ω model at 45°

Figure 78: Cross-sectional turbulent viscosity (ν_t) field for tested turbulence models at 45°

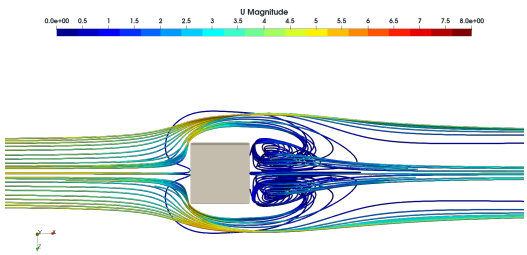

(a) U stream-lines, STD k-ϵ, at 0°

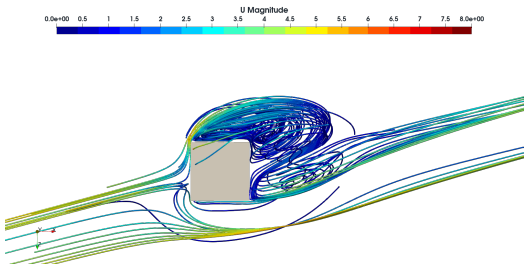

(b) U stream-lines, STD k-ϵ, at 15°

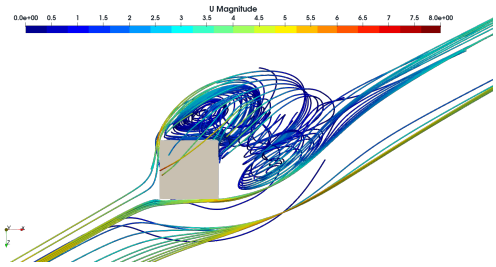

(c) U stream-lines, STD k-ϵ, at 30°

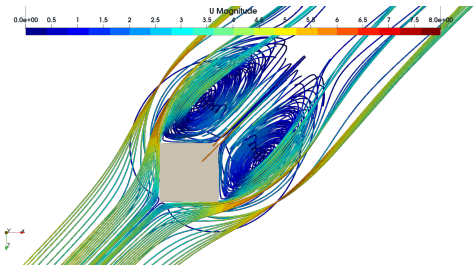

(d) U stream-lines, STD k-ϵ, at 45°

Figure 79: U stream-lines, STD k-ϵ

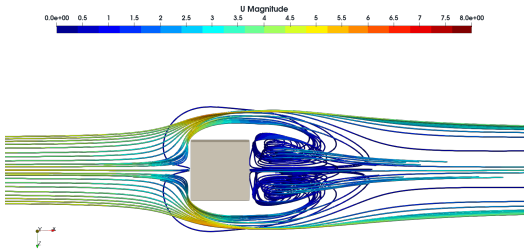

(a) U stream-lines, Realizable k-ϵ, at 0°

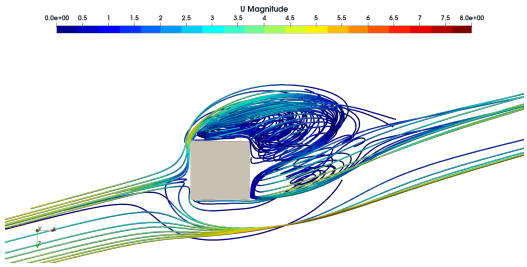

(b) U stream-lines, Realizable k-ϵ, at 15°

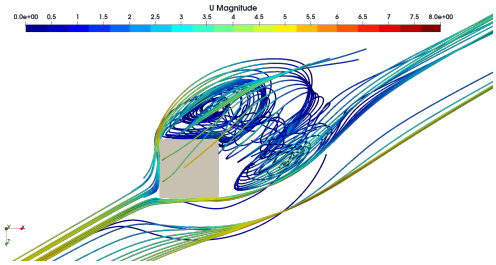

(c) U stream-lines, Realizable k-ϵ, at 30°

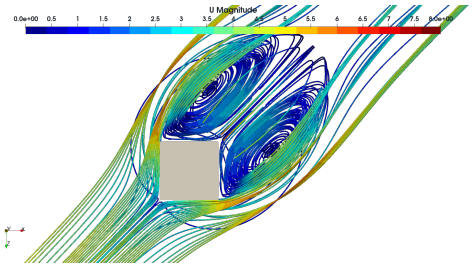

(d) U stream-lines, Realizable k-ϵ, at 45°

Figure 80: U stream-lines, Realizable k-ϵ

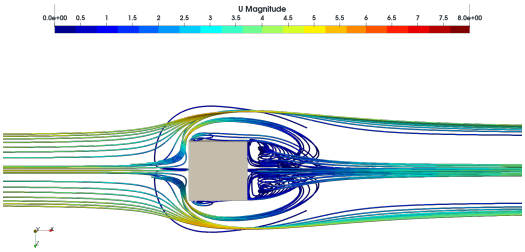

(a) U stream-lines, RNG k-ϵ, at 0°

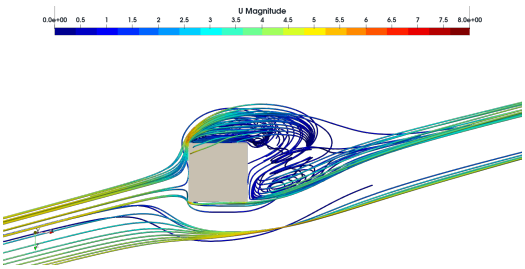

(b) U stream-lines, RNG k-ϵ, at 15°

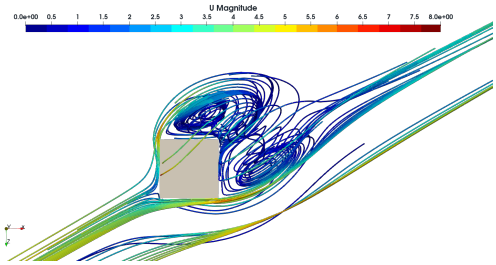

(c) U stream-lines, RNG k-ϵ, at 30°

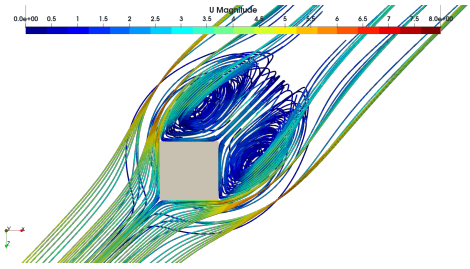

(d) U stream-lines, RNG k-ϵ, at 45°

Figure 81: U stream-lines, RNG k-ϵ

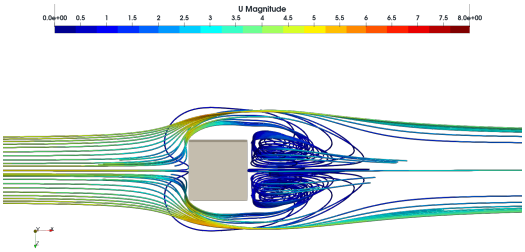

(a) U stream-lines, STD k-ω, at 0°

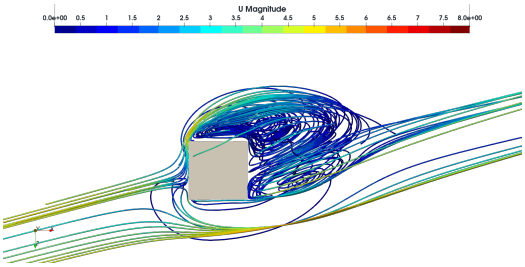

(b) U stream-lines, STD k-ω, at 15°

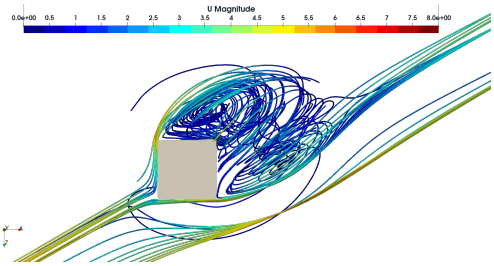

(c) U stream-lines, STD k-ω, at 30°

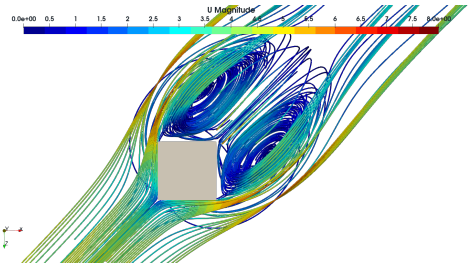

(d) U stream-lines, STD k-ω, at 45°

Figure 82: U stream-lines, STD k-ω

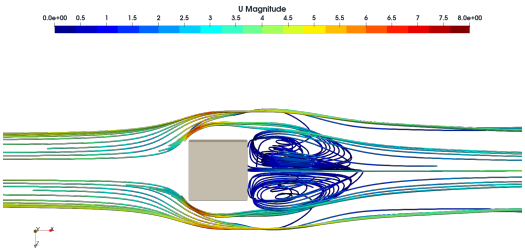

(a) U stream-lines, SST k-ω, at 0°

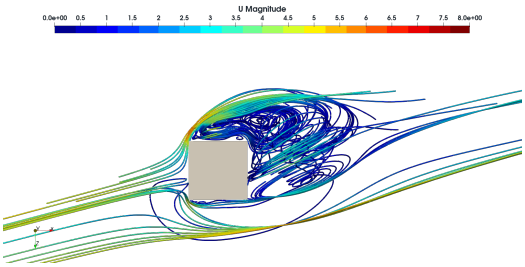

(b) U stream-lines, SST k-ω, at 15°

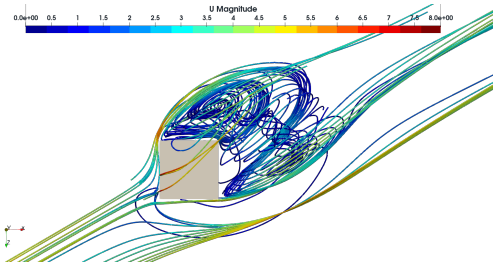

(c) U stream-lines, SST k-ω, at 30°

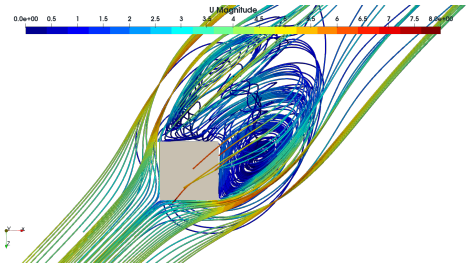

(d) U stream-lines, SST k-ω, at 45°

Figure 83: U stream-lines, SST k-ω

3. Acknowledgements.

The author acknowledges the financial support provided by the Secretaría de Ciencia, Humanidades, Tecnología e Innovación (SECIHTI, México) through a doctoral scholarship, which funded the author's full period of doctoral studies. This support is gratefully appreciated and contributed significantly to the completion of the research reported in this electronic supplementary material.